

RSC Advances



This is an *Accepted Manuscript*, which has been through the Royal Society of Chemistry peer review process and has been accepted for publication.

Accepted Manuscripts are published online shortly after acceptance, before technical editing, formatting and proof reading. Using this free service, authors can make their results available to the community, in citable form, before we publish the edited article. This *Accepted Manuscript* will be replaced by the edited, formatted and paginated article as soon as this is available.

You can find more information about *Accepted Manuscripts* in the [Information for Authors](#).

Please note that technical editing may introduce minor changes to the text and/or graphics, which may alter content. The journal's standard [Terms & Conditions](#) and the [Ethical guidelines](#) still apply. In no event shall the Royal Society of Chemistry be held responsible for any errors or omissions in this *Accepted Manuscript* or any consequences arising from the use of any information it contains.

Surface-Initiated ATRP of Styrene from Epoxy Groups of Graphene Nanolayers: Twofold Polystyrene Chains and Various Graft Densities

Hossein Roghani-Mamaqani

Department of Polymer Engineering, Sahand University of Technology, P.O. Box 51335-1996, Tabriz, Iran.

ABSTRACT

An initiator and amine group containing modifier, N-(2-aminoethyl)-2-bromo-2-methylpropanamide (OBr), was synthesized through the coupling reaction of ethylenediamine and alpha-bromoisobutyryl bromide. Subsequently, graphene oxide (GO) was functionalized with OBr in different densities by ring opening of epoxy groups. Then, the initiator-anchored graphene (GOBr) was used in different amounts as the precursor for grafting from atom transfer radical polymerization of styrene. Grafting of OBr on GO was approved by X-ray photo electron spectroscopy, elemental analysis, and Fourier transform infrared spectroscopy. The crystal structure of carbon and also stacking order of nanolayers were studied by Raman spectroscopy. The expansion of graphene interlayer by oxidation and modification processes was confirmed by X-ray diffraction. Conversion values were obtained from gas chromatography results. Free and attached polystyrene (PS) chains were deeply characterized by molecular weight and PDI values

using size exclusion chromatography. Molecular weight and PDI values of free chains are lower than the attached chains. Thermogravimetric analysis was also used to investigate the degradation temperatures, char contents, grafting weight ratios, and grafting molar ratios for modifier and PS chains. Graphene nanolayers confinement effect on the relaxation of PS chains was evaluated by differential scanning calorimetry. T_g values increased by increasing graphene content and grafting density. Scanning electron and transmission electron microscopies show that graphene nanolayers are flat, GO nanolayers are wrinkled, and PS-attached nanolayers are opaque because of polymer grafting.

KEYWORDS: Surface-initiated ATRP, Polystyrene, Graphene nanoplatelets, Epoxy groups, Graft density

INTRODUCTION

Graphene-based polymer nanocomposites have been an interesting subject in the past few decades, because of excellent characteristics and inexpensive source of graphene. Graphene are composed of sp^2 -hybridized carbon atoms in a honeycomb structure. These nanolayers are stacked because of strong π - π interaction between them. Consequently, graphene functionalization is inevitable in polymer grafting reactions. Chemical oxidation and exfoliation of graphite is a convenient method to prepare graphene nanolayers with various oxygen-containing functional groups, known as graphene oxide (GO). Hydroxyl and epoxy in the basal plane and carboxyl at the edges of GO can be used as the precursor to graft polymer chains by esterification, acylation, silane grafting, or epoxy ring opening reactions [1-6]. Polymer grafting is mainly accomplished by three methods of “grafting from”, “grafting through”, and “grafting

to” [1]. In “grafting from”, polymer chains initiate from the anchored initiator moieties on a substrate. In “grafting through”, polymer grafting is possible through the engagement of macroradicals with double bonds on a substrate. In “grafting to”, the pre-synthesized polymer chains are attached onto a substrate via coupling reactions. Grafting polymer chains from the initiator moieties anchored to a substrate results in the highest grafting density [2].

Well-defined polymers have commonly been synthesized by controlled radical polymerization (CRP). Among various CRP approaches, atom transfer radical polymerization (ATRP), which is based on reversible termination of growing radicals by a halogen atom, has been used numerous times in the synthesis of macromolecules with predetermined molecular weight. Polymer grafting of graphene nanolayers using CRP has frequently been carried out from the surface and edge functional groups using various grafting methods. Considering grafting through reactions from hydroxyl groups, we used 3-(trimethoxysilyl)propyl methacrylate (MPS) in different contents to functionalize GO in various graft densities. Then, polymerization of styrene was accomplished in the presence of MPS-modified GO [7]. MPS was also used by Tan et al. in a similar way to conduct the grafting through polymerization of poly(styrene-co-methyl methacrylate) [8]. In the case of edge carboxyl functional groups, Lo et al. also grafted glycidyl methacrylate at the edge of GO by an esterification reaction and subsequently anchored PNIPAAm chains at the edges [9]. We also coupled (3-methacryloxypropyl)dimethylchlorosilane (MCS) and 1,4-butanediol to prepare the modifier of GO from the edge carboxylic groups for use in grafting through reaction of polystyrene (PS) in various graft densities [10]. Considering grafting reactions from the surface hydroxyl groups, Lee et al. propagate PS, poly (methyl methacrylate) (PMMA), and poly (butyl acrylate) chains from the surface of alpha-bromoisobutyryl bromide (BiBB)-functionalized graphene [2]. Zhu et

al. directly attached BiBB to the surface of GO and subsequently synthesized thermoresponsive poly(N-isopropylacrylamide) (PNIPAAm) chains [11]. Our research group attached PS chains from the hydroxyl groups of GO using BiBB with various graft densities [12, 13]. Surface epoxy groups of GO were also used in grafting from reactions. Deng et al. reported the attachment of PNIPAAm chains with controlled grafting via *in situ* single-electron transfer living radical polymerization (SET-LRP) at the surface of graphene [9]. They also attached poly(ethylene glycol) ethyl ether methacrylate chains from the surface of GO similar to this procedure [14]. Other grafting reactions from the surface are also reported. Fang et al. anchored PS chains via diazonium and ATRP initiator introduction to the reduced GO surface [15]. They also carried out controlled grafting of PS chains from the surface of initiator-functionalized graphene [16]. Chen et al. used SET LRP to link poly (tert-butyl methacrylate) at the surface of graphene [17]. Ou et al. attached PMMA chains from the surface of BiBB-functionalized graphene. They functionalized GO with phenol groups by a 1,3-dipolar cycloaddition reaction at first [18]. Grafting polymer chains from the edge carboxyl functional groups of GO were also reported. Concalves et al. used BiBB-functionalized graphene nanoplatelets for grafting PMMA from the edges [19]. Also Ren et al. used the similar procedure for grafting PS and PMMA [20]. Yang et al. converted the carboxyl groups of GO to amine functionality by reacting with 1,3-Diaminopropane and prepared GO nanoplatelets with hydroxyl and amine groups. Then, poly(2-(dimethylamino)ethyl methacrylate) was grown from the BiBB-attached hydroxyl and amine groups [21]. Our research group also grafted PS chains from the edge carboxylic groups with various graft densities. Butanediol was used as coupling agent between the carboxylic groups and BiBB moieties [3].

Grafting reactions from the hydroxyl and carboxyl groups of GO in various graft densities were conducted by our research group. In this study, we carried out the grafting of PS from the epoxy groups in various grafting densities. Therefore, a bifunctional modifier with ATRP initiator and amine group moieties is synthesized and then attached on the surface of GO by an epoxy ring opening reaction. Subsequently, ATRP of styrene in the presence of functionalized graphene has been accomplished. PS chains are grown from the surface of graphene by a grafting from reaction in various grafting densities. Attachment of ATRP initiator and PS to the surface of graphene and effect of graft density on the kinetics, structure, and also thermal properties of the products are fully investigated. Designation of samples is given in Table 1.

Table 1

2. EXPERIMENTAL SECTION

Materials

Graphite was purchased from Merk, Germany. Styrene (Aldrich, 99%) was passed through an alumina-filled column, dried over calcium hydride, and distilled under reduced pressure (60 °C, 40mmHg). Copper(I) bromide (CuBr, Aldrich, 98%) was washed with glacial acetic acid, filtered, and finally washed with ethanol; it was dried under vacuum oven (50 °C, 40 mmHg) and then stored in a nitrogen atmosphere. N,N,N',N'',N''-pentamethyldiethylenetriamine (PMDETA, Aldrich, 99%), ethyl alpha-bromoisobutyrate (EBiB, Aldrich, 97%), alpha-bromoisobutyryl bromide (BiBB, Aldrich, 97%), anisole (Aldrich, 99%), ethylene diamine (EDA, Sigma-Aldrich, 99%), triethylamine (TEA, Sigma-Aldrich, 99%), N,N'-Dicyclohexylcarbodiimide (DCC, Aldrich, 99%), Potassium permanganate (KMnO₄, Sigma-Aldrich, 99%), Sodium nitrate (NaNO₃, Sigma-Aldrich, 99%), neutral aluminum oxide (Al₂O₃, Aldrich), N,N-

Dimethylformamide (DMF, Sigma, 99%), and Sulfuric acid (H₂SO₄, Merck) were used as received.

Characterization

¹H NMR (300 MHz) spectra were recorded on a Bruker Avance 300 spectrometer using CDCl₃ as the solvent and tetramethylsilane as the internal standard. A pulse delay of 1 s was used to ensure complete relaxation of spins.

X-ray photoelectron spectroscopy (XPS) was carried out on a Gammatdata-Scienta Esca 200 hemispherical analyzer equipped with an Al K α (1486.6 eV) x-ray source.

Elemental analysis (EA) was carried out with an Elementar Vario max CHNO Analyser (Hanau, German). Total carbon, hydrogen, nitrogen, and oxygen were determined by dry combustion method.

Fourier transform infrared (FTIR) spectra were recorded on a Bomem FTIR spectrophotometer within a range of 500–4000 cm⁻¹ using a resolution of 4 cm⁻¹. An average of 32 scans has been reported for each sample. The cell pathlength was kept constant during all the experiments. The samples were prepared on a KBr pellet in vacuum desiccators under a pressure of 0.01 torr.

Gas chromatography (GC) was performed on an Agilent-6890N with a split/splitless injector and flame ionization detector (FID), using a 60 m HP-INNOWAX capillary column for the separation. The GC temperature profile included an initial steady heating at 60 °C for 10 min. and a 10 °C/min ramp from 60 to 160 °C. The samples were also diluted with acetone. The ratio of monomer to anisole at different stages of the reaction was measured by GC to calculate monomer conversion throughout the reaction.

The average molecular weight and molecular weight distributions were measured by size exclusion chromatography (SEC) technique. A Waters 2000 ALLIANCE with a set of three

columns of pore sizes of 10000, 1000, and 500 Å was utilized to determine polymer average molecular weights and polydispersity index (PDI). THF was used as the eluent at a flow rate of 1.0 mL/min, and the calibration was carried out using low polydispersity PS standards. For the SEC measurements, catalyst particles were removed by passing the polymer solutions through a neutral aluminum oxide column.

X-ray diffraction (XRD) spectra were collected on an X-ray diffraction instrument (Siemens D5000) with a Cu target ($\lambda=0.1540$ nm) at room temperature. The system consists of a rotating anode generator, and operated at 35 kV and a current of 20 mA. The samples were scanned from 2 to 40° at the step scan mode, and the diffraction pattern was recorded using a scintillation counter detector. The basal spacing of the samples was calculated using the Bragg's equation.

Raman spectra were collected in the range from 3800 to 100 cm^{-1} using Bruker Dispersive Raman Spectrometer fitted with a 785 nm laser source, a CCD detector, and a confocal depth resolution of 2 μm . The laser beam was focused on the sample using an optical microscope.

Thermal gravimetric analyses were carried out with a PL thermo-gravimetric analyzer (Polymer Laboratories, TGA 1000, UK). The thermograms were obtained from ambient temperature to 550 °C at a heating rate of 10 °C/min. A sample weight of about 10 mg was used for all the measurements, and nitrogen was used as the purging gas at a flow rate of 50 ml/min; an empty pan was used as the reference.

Thermal analysis was carried out using a differential scanning calorimetry (DSC) instrument (NETZSCH DSC 200 F3, Netzsch Co, Selb/Bavaria, Germany). Nitrogen at a rate of 50 ml/min was used as the purging gas. Aluminum pans containing 2–3 mg of the samples were sealed using the DSC sample press. The samples were heated from ambient temperature to 220 °C at a heating rate of 10 °C/min. T_g was obtained as the inflection point of the heat capacity jump.

A Vega Tescan SEM analyzer (Czech Republic), was used to evaluate the morphology of the neat and modified graphenes which were gold-coated using a sputtering coater. The specimens were prepared by coating a thin layer of graphenes on a mica surface using a spin coater (Modern Technology Development Institute, Iran).

The transmission electron microscope, Philips EM 208, with an accelerating voltage of 120 kV was employed to study the morphology of the PS-attached graphenes.

Preparation of GO and graphene from graphite

GO was prepared using modified Hummers' method [22]. 1.5 g NaNO_3 and 3.0 g graphite powder were poured into a 300-mL three-necked flask which was placed in an oil bath. Then, 180 mL of H_2SO_4 was added into the reactor. The mixture was stirred for 15 min in the room temperature and then 9.0 g KMnO_4 was slowly added into the mixture till the temperature remains under 20 °C. Subsequently, temperature was increased to 35 °C and stirring was continued for 7 h. Then, 9.0 g KMnO_4 was added into the reactor and stirring was continued for additional 12 h at 35 °C. The reactor content was diluted by 600 mL deionized water. 30 mL of 30% H_2O_2 was poured into the diluted product to reduce the unreacted KMnO_4 . After centrifugation and washing the product with hydrochloric acid solution (1/10 with respect to water), wet GO washed three times with distilled water till its pH reaches to about 7. Then, graphite oxide dispersion (0.1 mg/mL) was exfoliated by water bath ultrasonication for 1 h. Finally, dried GO powder was obtained by filtration and vacuum at 65 °C. To obtain the graphene as reference GO was reduced by hydrazine: Yellow to brown dispersion of GO (100 mg) in water (100 mL) was ultrasonically agitated for 3 h. The dispersion was added into a 2-necked balloon which was placed in oil bath at 100 °C and equipped with a condenser. Then, hydrazine hydrate (1 mL) was added into the balloon. After 24 h, a black precipitate was

obtained after filtration. The filtrate was washed 5 times by distilled water (100 mL) and ethanol (100 mL). Finally, graphene nanoplatelets were obtained by vacuum oven at 65 °C.

Synthesis of N-(2-aminoethyl)-2-bromo-2-methylpropanamide (OBr)

Coupling reaction between the BiBB and EDA has performed as follows referring to literature [23]: EDA (30.05 g, 0.5 mol), TEA (16 mL, 0.114 mmol), and 250 mL DMF was poured into 500 mL three-necked jacketed lab reactor and left under purging with N₂ for 15 min. After setting the temperature at 0 °C, BiBB (10.8 g, 0.05 mol) in 100 mL DMF was added dropwise to the reactor and stirring was continued overnight at the room temperature. The obtained liquid was separated from the solid filtrates by filtration and then left in oven to evaporate the solvent. Then, 200 mL deionized water was added to the obtained liquid and the final product was extracted by chloroform. Then, the organic phase was separated and dried by MgSO₄. Distillation in vacuum yields a light yellow liquid with molecular weight of 209 g.mol⁻¹.

¹H NMR (in CDCl₃): δ 1.87 (s, 6H, (CH₃)₂), 2.80 (t, 2H, CH₂), 3.62 (t, 2H, CH₂).

Functionalization of GO by OBr

Coupling reaction between the epoxied functional groups of GO and amine groups of OBr was carried from the edge of GO referring to the literature [24]. GO (0.5 g) was dispersed in 150 mL DMF and after stirring for 2 h, ultrasonically agitated for 30 min to reach a homogeneous suspension. Subsequently, OBr (1.139 g for high graft density and 0.228 g for low graft density sample) in 50 mL DMF was added to the GO dispersion dropwise and stirring was continued to reach a homogeneous brown solution. Subsequently, DCC (0.25 g) was added into the reactor during 20 min and left under stirring for 24 h to yield a black product. After addition of 50 mL DMF to the reactor content, it was filtered through a 0.2 μm PTFE filter. The filtrate was washed 4 times with 200 mL ethanol to remove the unreacted OBr molecules. After drying the filtrate in

oven at 60 °C, OBr functionalized graphene nanolayers with various graft densities (GOBrL and GOBrH) were obtained.

Preparation of graphene/PS nanocomposites

ATRP reactions were performed in a 150-mL lab reactor which was heated by an oil jacket thermostated at 110 °C. A number of batch polymerizations were run in a solution medium with the molar ratios of 100:1:1:1 for [M]:[EBiB]:[CuBr]:[PMDETA]. The reactor was degassed and back-filled with nitrogen gas three times, and then left under N₂. Batch experiments were run by adding deoxygenated monomer (styrene, 30 mL), GOBr, catalyst (CuBr, 0.188 g), ligand (PMDETA, 0.274 mL), diluent (DMF, 10 mL), and 0.5 mL of deoxygenated anisole as internal standard to the reactor and then increasing the reaction temperature to 110 °C. The solution turned light green as the CuBr/PMDETA complex formed. Finally, after the majority of the metal complex had formed, free initiator (EBiB, 0.96 mL) was added to the system to start the polymerization. A sample was taken before the reaction started and used as a reference to measure the conversion.

Separation of PS-attached graphenes

Nanocomposites were dissolved in DMF. Then, by high-speed ultracentrifugation and passing the solution through a 0.2 mm filter, the unattached polymer chains were separated from the anchored ones via passing through the filter pores. Washing the filter in DMF and exposing the solution to the air yields PS-attached graphenes. To separate the attached PS chains, NaOH (2 g), DMF (50 mL), and PS-attached graphene (50 mg) were poured into a balloon equipped with a condenser. After agitation for 72 h at 65 °C and passing the solution through a 0.2 mm filter, the solution poured into ethanol to precipitate PS chains. Finally, the attached chains were dried in oven at 60 °C.

Figure 1

3. RESULTS AND DISCUSSION

Graphite was used to prepare GO by an oxidation reaction. As shown in Figure 1, coupling reaction of ethylenediamine and BiBB yields OBr with functional groups of amine and ATRP initiator. Subsequently, GO was functionalized with OBr from epoxy groups to obtain initiator containing graphene (GOBr). Finally, GOBr was used in different weight percents as the precursor for ATRP of styrene.

The surface chemical composition of GO and GOBrH were monitored by XPS. Figure 2 (A) shows the XPS full-scan spectra of GO and GOBrH and also the higher resolution spectra for N_{1s} and Br_{3d} . The survey scan spectrum of GO is dominated by peaks assigned to oxygen (O_{1s}) and carbon (C_{1s}). Appearance of N_{1s} and Br_{3d} bands in the spectrum of GOBrH at the binding energy of about 401.5 and 74-78 eV originates from the covalent attachment of OBr at the surface of GO [25, 26]. Br_{3d} core-level spectrum for GOBrH at the binding energy of 74-78 eV can be curve-fitted with two peak components at binding energies of about 74.2 (Br $3d_{5/2}$) and 77.0 eV (Br $3d_{3/2}$) [13, 27]. Increase of C_{1s} peak area after modification with OBr shows partial reduction of GO. The C_{1s} band spectrum of GOBrH is deconvoluted to investigate the type and amount of various carbon-containing functional groups (Figure 2 (B)). Functional groups of carbonyl, carboxyl, epoxy, and hydroxyl are formed upon the oxidation of graphene [2, 3]. Also, appearance of C–Br and C–N peaks at 287.5 and N–C=O peak at 289.1 eV clearly confirms the successful grafting of OBr on the epoxy functional groups. The difference between the sum of C–N and C–Br peak area and O=C–N results from the graphene grafted ED moieties which do not participate in the reaction with BiBB. The content of each functional group from the ratio of peak area in the deconvoluted C_{1s} spectra and the results of elemental analysis for GO [10],

GOBrL, and GOBrH are presented in Table 2. After OBr modification of GO, reduction of the carbonyl and carboxyl peaks area, increase of graphitic carbon bonds peak area from XPS results, and also increase of C/O ratio from elemental analysis results show the reduction of GO during the modification process [27, 28]. Replacement of epoxy groups with nitrogen atoms of ED also results in a low content of C–O–C groups in GOBrH. A comparison of nitrogen content between the GOBrL and GOBrH in elemental analysis data shows that higher amount of epoxy functional groups is reacted with OBr in the case of GOBrH. After the modification process, C/O ratio is increased from 0.69 to 2.95 which clearly shows the partial reduction of GO nanolayers. The higher C/O ratio for GOBrH is also an indication of its higher reduction compared with GOBrL.

Figure 2

Table 2

Figure 3 (A) shows the FTIR spectra for graphene, GO, OBr, GOBrL, GOBrH, PS, and its nanocomposites with various graft densities. Hydroxyl and carboxyl stretching vibrations at 3398 and 1716 cm^{-1} and also epoxy groups vibration at 853 and 1051 cm^{-1} are appeared after oxidation of graphene [12, 29]. Additionally, OH-stretching vibration 3414 cm^{-1} is intensified because of the presence of hydroxyl groups and also water adsorption. OBr shows C–H vibration in methyl or methylene groups at 2861 and 2930 cm^{-1} , methylene C–H bending vibration at 1424 cm^{-1} , in-plane bending vibration of vinyl C–H at 1381 cm^{-1} [30], N–H stretching and bending vibrations at 3440 and 1493 cm^{-1} [31], amide carboxyl stretching vibration at 1661 cm^{-1} . Attachment of OBr in GOBrL and GOBrH is confirmed by appearance of N–H stretching vibration at 3321 cm^{-1} , C–H stretching vibration at 2849 and 2923 cm^{-1} , and also intensified stretching vibration of N–C=O stretching vibration at 1624 cm^{-1} . Also, in high graft density OBr functionalized graphene,

the intensity of these peaks are larger. Also, the C–Br vibration seen at 790 cm^{-1} in GCBrL and GCBrH patterns clearly shows that modification process was carried out successfully [32]. PS and its nanocomposites show some characteristic peaks of C–H stretching vibration of methylene groups and stretching vibration of non-conjugated carbon–carbon double bonds at 2911 and 1593 cm^{-1} which are related with PS backbone. PH3 and PL3 shows N–C=O stretching vibration at 1661 cm^{-1} and N–H vibration at 1593 cm^{-1} , which are confirmations of grafting of polymer chains on OBr modified graphenes. C–Br bond vibration at 746 cm^{-1} is also an indication of chain end functionality of PS chains [32].

Raman spectroscopy was used to characterize the crystal structure of carbon for all the graphenes. Raman spectra for G, GO, GOBrL, GOBrH, PL3A, and PH3A are displayed in Figure 3 (B). G has three major peaks of D-band at 1313 , G-band at 1577 , and 2D or G'-band at 2641 cm^{-1} . D-band (breathing mode of κ -point phonons of A_{1g} symmetry) originates from defects inherent in graphene (disorder), G-band (in-plane bond stretching motion of the sp^2 C atoms, E_{2g} mode) arises from aromatic domains (order), and 2D-band originates from the stacking order of nanolayers [33, 34]. Generally, a perfect graphene crystal does not show the D-band; however, because of the high temperature treatments during the production, most of the industrial graphenes show this peak [35]. The G-band of GO appeared at higher wave numbers in comparison with graphene, 1589 cm^{-1} . Interestingly, after functionalization of GO with OBr and PS, the G-band wave number shifts back to the pristine graphene's G-band wave number (about 1579 cm^{-1} for all the OBr- and PS-functionalized graphenes). This shows that the electric conjugation within the graphitic network is restored to some extent after grafting of OBr or PS [36]. The 2D-band is the second order of the D-band. It is commonly used to study the stacking of graphene nanolayers. This is a single symmetrical peak in monolayer graphene, whereas it

splits in four bands in bilayer graphene [37]. Additionally, it has a shoulder in the case of graphite. Depending on the number of layers, an intermediate shape is obtained for the multilayer graphene [37, 38]. Disappearance of 2D-band in the spectrum of the modified graphenes shows that stacking order is reduced and exfoliated state may be achieved [10, 3].

Figure 3

XRD is used for evaluation of the extent of graphene nanolayers expansion and the results are presented in Figure 4 (A) and (B). Graphene interlayer distance increases from 0.34 to 0.94 nm after oxidation which corresponds to a decrease of diffraction angle from 26° to 9.45° (attributed to (002) plane of graphene nanolayers). GO also shows a weak and broad peak at a diffraction angle of 19.33° , which indicates the presence of oxygen-containing functional groups formed upon the oxidation process [15, 17]. The diffraction angle of about 8.25° for the OBr-grafted graphenes shows that the interlayer distance is further increased by anchoring the initiator-containing functional groups from the graphene surface. Disappearance of the diffraction peaks of G and GO in the modified graphenes shows that the nanolayers are fully expanded by the oxidation and modification processes. Interestingly, amine-modification results in partial reduction of GO and appearance of a peak at 26.85° for both of GOBrL and GOBrH [35]. The intensity of this peak is higher for GOBrH, which is on account of a higher amount of amine modification. According to Figure 4 (B), nanocomposites show a broad amorphous shallow diffraction peak resulting from their amorphous structure [10, 39]. Polymerization initiates from the initiator moieties on the surface of modified graphenes. Subsequently, nanolayers are pushed apart by propagation of PS chains on the surface. Diffraction patterns of all the nanocomposites with various grafting densities are similar, which shows that interlayer distance expansion can be achieved by smaller amounts of PS chains.

Figure 4

GPC traces for the free and attached PS chains are monitored in Figure 5 (A), (B). The extracted data from the traces in combination with the conversion values are also companied. According to the results, conversion values are increased by increasing graphene content and grafting density of OBr moieties. This shows that modified graphene exerts an acceleration effect on the polymerization of styrene, which is mainly on account of its oxygen-containing functional groups [3, 13, and 40]. A large number of oxygen-containing groups of GO after modification with OBr inserts a polarizing effect and consequently increase the polymerization rate. Although the higher graft densities of OBr reduce the amount of oxygen-containing polar groups of modified graphene, but the effect of neighbor active heads results in higher conversion values. Addition of OBr-modified graphene results in the free and attached PS chains with various characteristics. By increasing modified graphene content, the proportion of attached initiator moieties increased; therefore, both of the free and attached chains molecular weights are decreased. The effect of neighbor active heads, which is known as viscose region, results in attached chains with higher molecular weights than the free chains [3, 41]. A large number of dormant chains end are present in the viscose region which results in the rapid diffusion of activator species with smaller size compared with the deactivator molecules with larger size. Consequently, higher concentration of catalyst in the lower oxidation state in this region results in higher polymerization rate. The effect of viscose region is intensified in higher grafting densities. Therefore, increase of grafting densities results in attached chains with higher molecular weights. Consequently, the molecular weights of free chains are decreased. Addition of graphene content and grafting density results in higher PDI values of attached and free chains. However, PDI values of attached chains are higher than the free ones. This is mainly on account

of the small distance between the growing radicals and their higher probability of combination reactions. Molecular weight of free chains decreases by increasing modified graphene content and also grafting density. Consequently, PDI values of free chains are lower than the attached PS chains.

Figure 5

Figure 6

Thermal characteristics of the samples are evaluated by TGA and the thermograms of weight loss as a function of temperature for the G, GO, OBr and PS-modified graphenes, and also nanocomposites are presented in Figure 6 (A-D). Figure 6 (A) shows a small mass loss below 150 °C for GO which is resulted from stored water in its π -stacked structure [42, 43]; however, G is stable to a large state till 550 °C (93.2 wt% char value). By substitution of OBr moieties with the polar oxygen-containing groups (epoxy groups) at the surface in GOBrL and GOBrH, the extent of the absorbed water decreases. Interestingly, the amount of absorbed water in GOBrH is a bit lower than GOBrL because of its higher grafting density of OBr moieties. GO reveals a two-step major weight loss. The first one, between 150 and 220 °C, is a result of CO, CO₂, and steam release from the most labile functional groups. The second one, between 220 and 550 °C, is attributed to degradation of more stable oxygen functional groups [44, 45]. Finally, GO reaches to char value of about 40.5 wt% at 550 °C. However, a different decomposition thermogram is observed for GOBrL and GOBrH, which can be explained by the loss of epoxy groups at the surface of GO by the reaction with OBr. The thermogram of GOBrL is more similar to GO which is because of its low grafting density of OBr moieties and higher stable oxygen functional groups. Degradation of OBr and the remained oxygen-containing functional groups results in the char value of about 43.9 and 51.3 wt% for GOBrL and GOBrH. The weight

loss difference between the GO and OBr-modified graphenes (3.4 and 10.8 wt% for the low and high grafting density samples respectively) can be used as an estimation of grafted OBr. Additionally, OBr moieties retard decomposition of GO by decreasing the amount of oxygen-containing functional groups, according to the higher decomposition temperature of GOBrH and GOBrL with respect to GO. Figure 6 (B) shows the TGA thermograms for the high density nanocomposites. Accordingly, degradation temperature of all the nanocomposites is higher than the PS. There is not a considerable discrepancy between the char values of nanocomposites; however, a difference of about 3 wt% can be observed between the PS and its nanocomposites. This shows that even a very low content of modified graphene can improve thermal stability and increase char value of PS matrix to a considerable content. Figure 6 (C and D) show TGA curves for the PS-attached graphenes extracted from the high and low density nanocomposites respectively. Degradation of PS-attached graphenes consists of three steps. The first two steps relate to the decomposition of oxygen-containing groups of graphene and the third step relates to degradation of the attached PS chain. Table 3 shows some data derived from the TGA thermograms of GOBrL, GOBrH, and PS-attached graphenes. Degradation value at the third step decreases by increasing of graphene content as a result of lowering PS molecular weight. The weight and molar ratio of OBr and PS chains at the graphene surface can be calculated from TGA results using equations 1-4 [30, 46-49].

$$G_{r,OBr} (\text{weight ratio of OBr on graphene}) = \frac{w\%_{OBr}}{100 - w\%_{OBr}} \quad (1)$$

$$G_{r,PS} (\text{weight ratio of PS on graphene}) = \frac{w\%_{PS}}{100 - w\%_{PS}} - \frac{w\%_{OBr}}{100 - w\%_{OBr}} \quad (2)$$

$$G_{p,OBr} (\text{molar ratio of OBr on graphene}) = \frac{\left(\frac{w\%_{OBr}}{100 - w\%_{OBr}} \right)}{M_{OBr}} \quad (3)$$

$$G_{p,PS}(\text{molar ratio of PS on graphene}) = \frac{\left(\frac{w\%_{PS}}{100 - w\%_{PS}} - \frac{w\%_{OBr}}{100 - w\%_{OBr}} \right)}{M_{PS}} \quad (4)$$

where, $w\%_{OBr}$, $w\%_{PS}$, M_{OBr} (208.09 g/mol), and M_{PS} denote the weight losses and molecular weights for OBr and PS, respectively.

Table 3

Figure 7 shows DSC thermograms in the temperature range of 80–120 °C and T_g values for PS and its nanocomposites with various grafting densities. Effect of graphene content and grafting density on T_g value, enthalpy relaxation, and also ΔC_p near the T_g was evaluated by DSC. The curves were obtained after removing the thermal history. T_g is commonly increased by presence of confinements for relaxation of polymer chains. For example grafting of polymer chains on a substrate results in higher T_g values [15, 16]. In addition, molecular weight of polymers, density of grafting, size of substrate, loading value, and interactions between substrates and polymer chains are some other effective parameters on T_g [50-52]. Results show that T_g is increased by the addition of graphene content and also grafting density. This shows that PS chains are more confined by the addition of higher graphene content and also by their neighbors in the graft form in higher grafting densities. Graphene nanolayers exert considerable confinement on the relaxation of polymer chains because of their planar geometry. This can easily proved by increase of T_g value by about 22.7 °C at only 0.4 wt% loading (100.3 for PH4 against 77.6 °C for PS) [50, 51]. Also, enthalpy relaxation is increased in the T_g point by increasing graphene content. Heat capacity variations (ΔC_p) near the T_g are different in the case of PS and its nanocomposites with various grafting densities. The higher graphene contents and graft densities exhibit a higher heat flow step in T_g compared with the lower graphene contents and grafting densities, which may results from the decreased chain packing densities [7].

Figure 7

Figure 8 (A-D) displays SEM images for graphene, GO, GOBrH, and PH3A respectively. Size of graphene nanolayers varies from several hundred nanometers to ten micrometers. Bare and flat surface of graphene converted to wrinkled nanolayers with curvature after oxidation. The wrinkled structure is remained after functionalization of GO with OBr moieties. By covering PS, nanolayers with higher opacity are obtained. Figure 8 (E-G) displays TEM micrographs of graphene, GO, and PH3A. Graphene nanolayers loose their flat surface and transparency after oxidation and functionalization processes. Lots of creases and folding are observed for GO. PS attachment results in opaque nanolayers with low transparency as a result of the presence of polymeric chains. Figure 8 (H) shows the Dispersibility of graphene, GO, GOBrL, GOBrH, PL3A, and PH3A was evaluated in DMF just after sonication and 10 days after. Dispersibility and stability of GO is higher than the others which results from its high content of oxygen-containing functional groups. GOBrL and GOBrH because of the large amount of polar functional groups are dispersed appropriately and formed stable dispersions. However, PS attachment reduced the stability of their dispersions in DMF. This is predictable since the polarity of PS chains is not in the range of DMF. Stability of PH3A dispersion in DMF is lower than PL3A, which is also on account of higher PS chains grafted at the surface of graphene nanolayers.

Figure 8

4. CONCLUSIONS

Bifunctional modifier of OBr with ATRP initiator and amine group moieties was synthesized by coupling reaction of ethylenediamine and BiBB. Then, GO was functionalized with OBr in different densities by ring opening of epoxy groups. Subsequently, ATRP of styrene in the

presence of GOBr with different weight percents has been carried. Free initiator used as sacrificial agent; therefore, free and attached polymer chains are formed. Appearance of N_{1s} and Br_{3d} bands in the XPS spectrum of GOBrH respectively at the binding energy of about 401.5 and 74-78 eV originates from the covalent attachment of OBr at the surface of GO. Attachment of OBr is also confirmed by appearance of N–H, C–H, and intensified N–C=O stretching vibrations in FTIR patterns of GOBrL and GOBrH. Disappearance of XRD diffraction peaks of G and GO in the modified graphenes shows that the nanolayers are fully expanded by the oxidation and modification processes. By increasing modified graphene content, molecular weights of the free and attached chains are decreased. Increasing grafting density results in lower molecular weights of free chains. Addition of graphene content and grafting density results in higher PDI values of attached and free chains. Modifier content of 3.4 and 10.8 wt% for GOBrL and GOBrH shows that molar ratio of OBr is equals to 169.15 and 519.0 $\mu\text{mol/g}$ respectively. Higher graphene content and grafting densities results in higher T_g values. SEM and TEM images show that graphene nanolayers are flat, GO nanolayers are wrinkled, and PS-attached nanolayers are opaque because of polymer grafting.

ACKNOWLEDGMENTS

Iran National Science Foundation (INSF) is greatly appreciated for its financial support (Grant Number: 93030431).

REFERENCES

1. H. Roghani-Mamaqani, V. Haddadi-Asl, M. Salami-Kalajahi, *Polym. Rev.*, 2012, **52**, 142–188.

2. S. H. Lee, D. R. Dreyer, J. An, A. Velamakanni, R. D. Piner, S. Park, Y. Zhu, S. O. Kim, C. W. Bielawski, R. S. Ruoff, *Macromol. Rapid. Commun.*, 2010, **31**, 281–288.
3. H. Roghani-Mamaqani, V. Haddadi-Asl, K. Khezri, M. Salami-Kalajahi, *RSC Adv.*, 2014, **4**, 24439.
4. Q. Yang, X. Pan, K. Clarke, K. Li, *Ind. Eng. Chem. Res.*, 2012, **51**, 310–317.
5. H. Roghani-Mamaqani, V. Haddadi-Asl, Z. Sobhkhiz, M. Ghaderi-Ghahfarrokhi, *Colloid Polym. Sci.*, 2015, **293**, 735–750.
6. Y. Deng, J. Z. Zhang, Y. Li, J. Hu, D. Yang, X. Huang, *J. Polym. Sci.: Part A: Polym. Chem.*, 2012, **50**, 4451–4458.
7. H. Roghani-Mamaqani, V. Haddadi-Asl, K. Khezri, E. Zeinali, M. Salami-Kalajahi, *J. Polym. Res.*, 2014, **21**, 333.
8. Y. Tan, L. Fang, J. Xiao, Y. Song, Q. Zheng, *Polym. Chem.*, 2013, **4**, 2939–2944.
9. C.W. Lo, D. Zhu, H. Jiang, *Soft Matter*, 2011, **7**, 5604–5609.
10. H. Roghani-Mamaqani, V. Haddadi-Asl, K. Khezri, M. Salami-Kalajahi, *Polym. Int.*, 2014, **63**, 1912–1923.
11. S. Zhu, J. Li, Y. Chen, Z. Chen, C. Chen, Y. Li, Z. Cui, D. Zhang, *J. Nanopart. Res.*, 2012, **14**, 1132.
12. H. Roghani-Mamaqani, V. Haddadi-Asl, *Polym. Compos.*, 2014, **35**, 386–395.
13. H. Roghani-Mamaqani, V. Haddadi-Asl, K. Khezri, M. Salami-Kalajahi, M. Najafi, *Polym. Eng. Sci.*, 2015, DOI 10.1002/pen.24010.
14. Y. Deng, Y. Li, J. Dai, M. Lang, X. Huang, *J. Polym. Sci. Part A: Polym. Chem.*, 2011, **49**, 4747–4755.
15. M. Fang, K. Wang, H. Lu, Y. Yang, S. Nutt, *J. Mater. Chem.*, 2009, **19**, 7098–7105.

16. M. Fang, K. Wang, H. Lu, Y. Yang, S. Nutt, *J. Mater. Chem.*, 2010, **20**, 1982–1992.
17. X. Chen, L. Yuan, P. Yang, J. Hu, D. Yang, *J. Polym. Sci. Part A: Polym. Chem.*, 2011, **49**, 4977–4986.
18. B. Ou, Z. Zhou, Q. Liu, B. Liao, S. Yi, Y. Ou, X. Zhang, D. Li, *Polym. Chem.*, 2012, **3**, 2768–2775.
19. G. Goncalves, P. A. A. P. Marques, A. Barros-Timmons, I. Bdkin, M. K. Singh, N. Emami, J. Gracio, *J. Mater. Chem.*, 2010, **20**, 9927–9934.
20. L. Ren, X. Wang, S. Guo, T. Liu, *J. Nanopart. Res.*, 2011, **13**, 6389–6396.
21. Y. Yang, J. Wang, J. Zhang, J. Liu, X. Yang, H. Zhao, *Langmuir*, 2009, **25**, 11808–11814.
22. D. C. Marcano, D. V. Kosynkin, J. M. Berlin, A. Sinitskii, Z. Sun, A. Slesarev, L. B. Alemany, W. Lu, J. M. Tour, *ACS Nano*, 2010, **4**, pp 4806–4814.
23. C. Y. Hong, Y. Z. You, C. Y. Pan, *Chem. Mater.*, 2005, **17**, 2247–2254.
24. Y. Pan, H. Bao, N. G. Sahoo, T. Wu, L. Li, *Adv. Func. Mater.*, 2011, **21**, 2754–2763.
25. H. Datta, A. K. Bhowmick, N. K. Singha, *J. Polym. Sci.: Part A: Polym. Chem.*, 2008, **46**, 5014–5027.
26. Y. Sun, X. Ding, Z. Zheng, X. Cheng, X. Hu, Y. Peng, *Europ. Polym. J.*, 2007, **43**, 762–772.
27. Y. Chen, C. Wang, J. Chen, X. Liu, Z. Tong, *J. Polym. Sci.: Part A, Polym. Chem.*, 2009, **47**, 1354–1367.
28. S. H. Liao, P. L. Liu, M. C. Hsiao, C. C. Teng, C. A. Wang, M. D. Ger, C. L. Chiang, *Ind. Eng. Chem. Res.*, 2012, **51**, 4573–4581.
29. H. Roghani-Mamaqani, V. Haddadi-Asl, M. Mortezaei, K. Khezri, *J. Appl. Polym. Sci.*, 2014, **131**, 40273.

30. V. G. Ngo, C. Bressy, C. Leroux, A. Margaillan, *Polymer*, 2009, **50**, 3095–102.
31. E. Zeinali, V. Haddadi-Asl, H. Roghani-Mamaqani, *RSC Adv.*, 2014, **4**, 31428.
32. H. Roghani-Mamaqani, V. Haddadi-Asl, M. Najafi, M. Salami-Kalajahi, *Polym. Sci. Ser. B*, 2012, **54**, 153–160.
33. H. Hu, X. Wang, J. Wang, L. Wan, F. Liu, H. Zheng, *Chem. Phys. Lett.*, 2010, **484**, 247–253.
34. I. Y. Jeon, H. J. Choi, S. M. Jung, J. M. Seo, M. J. Kim, L. Dai, *J. Am. Chem. Soc.*, 2013, **135**, 1386–1393.
35. M. Nikdel, M. Salami-Kalajahi, M. Salami Hosseini, *Colloid Polym. Sci.*, 2014, **292**, 2599–2610
36. S. Sun, Y. Cao, J. Feng, P. Wu, *J. Mater. Chem.*, 2010, **20**, 5605–5607.
37. A. C. Ferrari, J. C. Meyer, V. Scardaci, C. Casiraghi, M. Lazzeri, F. Mauri, S. Piscanec, D. Jiang, K. S. Novoselov, S. Roth, A. K. Geim, *Phys. Rev. Lett.*, 2006, **97**, 187401–18744.
38. R. Sanna, D. Sanna, V. Alzari, D. Nuvoli, S. Scognamillo, M. Piccinini, *J. Polym. Sci., Part A: Polym. Chem.*, 2012, **50**, 4110–4118.
39. M. Li, Y. G. Jeong, *Composites: Part A*, 2011, **42**, 560–566.
40. H. Roghani-Mamaqani, V. Haddadi-Asl, K. Khezri, M. Salami-Kalajahi, M. Najafi, M. Sobani, S. A. Mirshafiei-Langari, *Iran. Polym. J.*, 2015, **24**, 51–62.
41. R. E. Behling, B. A. Williams, B. L. Staade, L. M. Wolf, E. W. Cochran, *Macromolecules*, 2009, **42**, 1867–1872.
42. I. Jung, D. Dikin, S. Park, W. Cai, S. L. Mielke, R. S. Ruoff, *J. Phys. Chem. C*, 2008, **112**, 20264–20268.
43. M. Nikdel, M. Salami-Kalajahi, M. Salami-Hosseini, *RSC Adv.*, 2014, **4**, 16743.

44. S. Stankovich, D. A. Dikin, R. D. Piner, K. A. Kohlhaas, A. Kleinhammes, Y. Jia, *Carbon*, 2007, **45**, 1558–1565.
45. J. Shen, Y. Hu, M. Shi, X. Lu, C. Qin, C. Li, *Chem. Mater.*, 2009, **21**, 3514–3520.
46. D. Hua, J. Tang, J. Jiang, Z. Gu, L. Dai, X. Zhu, *Mater. Chem. Phys.*, 2009, **114**, 402–406.
47. C. H. Liu, C. Y. Pan, *Polymer*, 2007, **48**, 3679–3685.
48. H. Roghani-Mamaqani, V. Haddadi-Asl, M. Ghaderi-Ghahfarrokhi, Z. Sobhkhiz, *Colloid Polym. Sci.*, 2014, **292**, 2971–2981.
49. H. Hemmatpour, V. Haddadi-Asl, H. Roghani-Mamaqani, *Polymer*, 2015, **65**, 143–153.
50. H. Roghani-Mamaqani, V. Haddadi-Asl, M. Najafi, M. Salami-Kalajahi, *AIChE J.*, 2011, **57**, 1873–1881.
51. L. Ahmadian-Alam, V. Haddadi-Asl, H. Roghani-Mamaqani, L. Hatami, M. Salami-Kalajahi, *J. Polym. Res.*, 2012, **19**, 9773.
52. K. Khezri, V. Haddadi-Asl, H. Roghani-Mamaqani, M. Salami-Kalajahi, *Polym. Compos.*, 2012, **33**, 990–998.

Table 1- Designation of the samples

Designation	Description
EDA	Ethylenediamine
BiBB	alpha-bromoisobutyryl bromide
OBr	N-(2-aminoethyl)-2-bromo-2-methylpropanamide
PS	Polystyrene
GO	Graphene oxide
GOBrL	Low density OBr-functionalized GO
GOBrH	High density OBr-functionalized GO
PLX	PS/GOBrL nanocomposite with 0.X wt% GOBrL
PHX	PS/GOBrH nanocomposite with 0.X wt% GOBrL
PLXA	Low density PS-functionalized graphene from the source PLX
PHXA	High density PS-functionalized graphene from the source PHX

Table 2- Surface functional groups compositions of GO and GOBrH from decomposition of the C_{1s} spectrum, and elemental composition from Elemental analysis

Graphene	Composition of C in groups						
	O=C-O	O=C-N	C=O	C-O-C C-O	C=C	C-C	C-N C-Br
GO	5.72	---	30.47	33.89	21.23	8.69	----
GOBrH	6.34	7.45	11.85	13.16	34.80	15.25	11.15
	Element (%)				Element Ratio		
	C	H	O	N	C/O	C/N	
G	95.3	1.8	2.9	---	32.86	---	
GO	39.7	2.4	57.9	---	0.69	---	
GOBrL	54.8	3.9	27.3	8.4	2.01	6.52	
GOBrH	62.8	4.2	21.3	9.7	2.95	6.47	

Table 3- Data derived from the TGA thermograms

Sample	Char value	Third step degradation	$G_{r,OBr} \times 10^2$	$G_{r,PS} \times 10^2$	$G_{p,OBr}$ ($\mu\text{mol/g}$)	$G_{p,PS}$ ($\mu\text{mol/g}$)
GOBrL	43.9	3.4	3.52	----	169.15	----
GOBrH	51.3	10.8	12.11	----	519.00	----
PL1A	34.1	31.5	----	42.46	----	29.45
PH1A	33.1	33.2	----	37.59	----	23.51
PL2A	37.0	30.8	----	40.98	----	----
PH2A	34.3	32.2	----	35.38	----	----
PL3A	36.4	29.9	----	39.13	----	34.60
PH3A	34.4	32.6	----	36.26	----	28.44
PL4A	38.2	26.3	----	32.16	----	----
PH4A	35.4	28.4	----	27.55	----	----

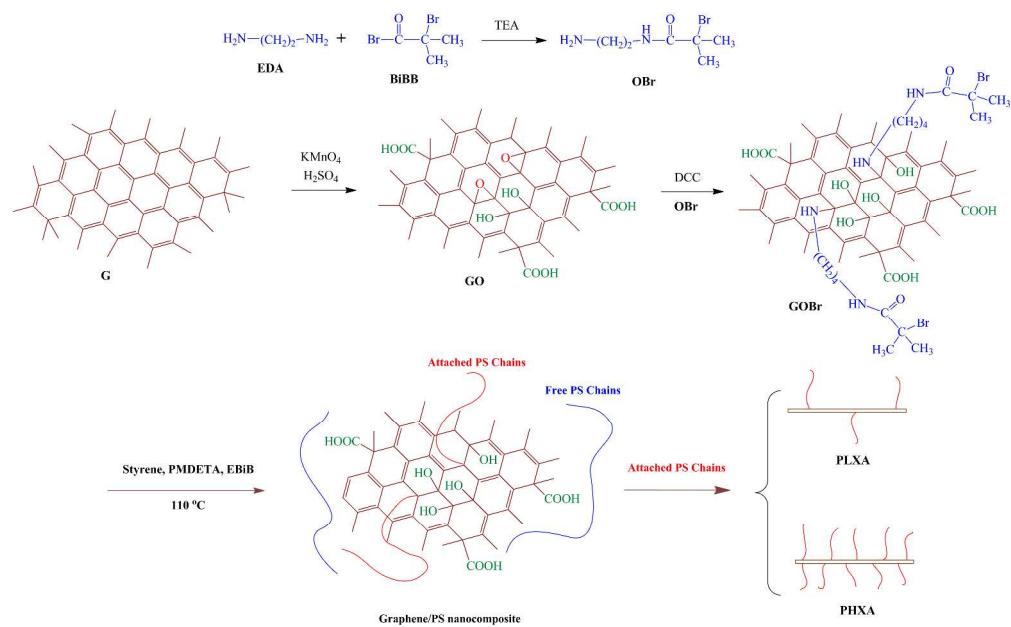


Figure 1- Synthesis of OBr, oxidation of graphene and its functionalization with OBr, and synthesis of PS-attached graphenes with various graft densities
391x240mm (300 x 300 DPI)

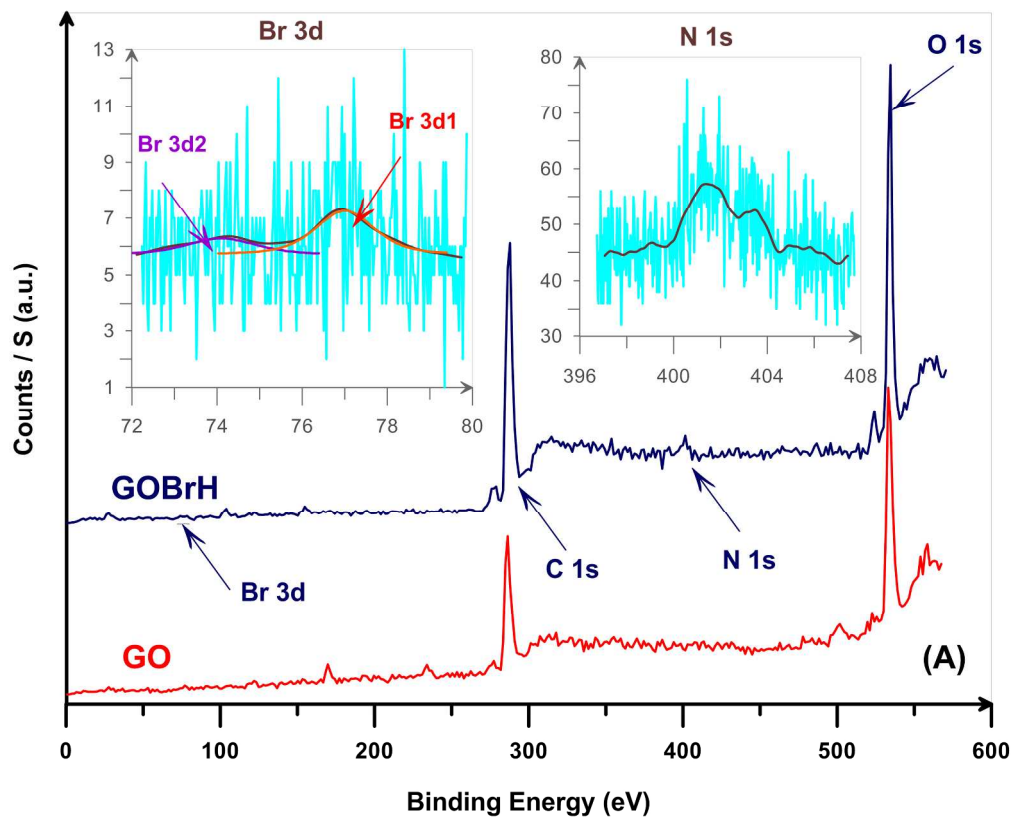


Figure 2- (A) Survey scan XPS for GO and GOBrH and (B) deconvoluted C1s core-level spectrum of GOBrH
687x558mm (96 x 96 DPI)

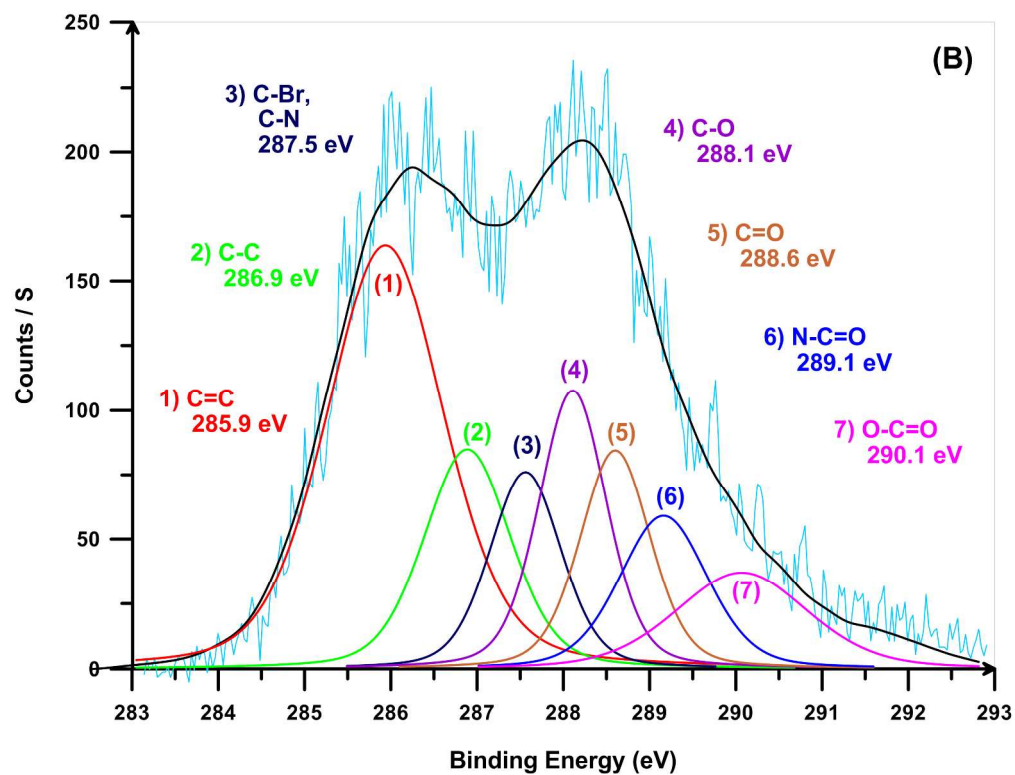


Figure 2- (A) Survey scan XPS for GO and GOBrH and (B) deconvoluted C1s core-level spectrum of GOBrH
737x561mm (96 x 96 DPI)

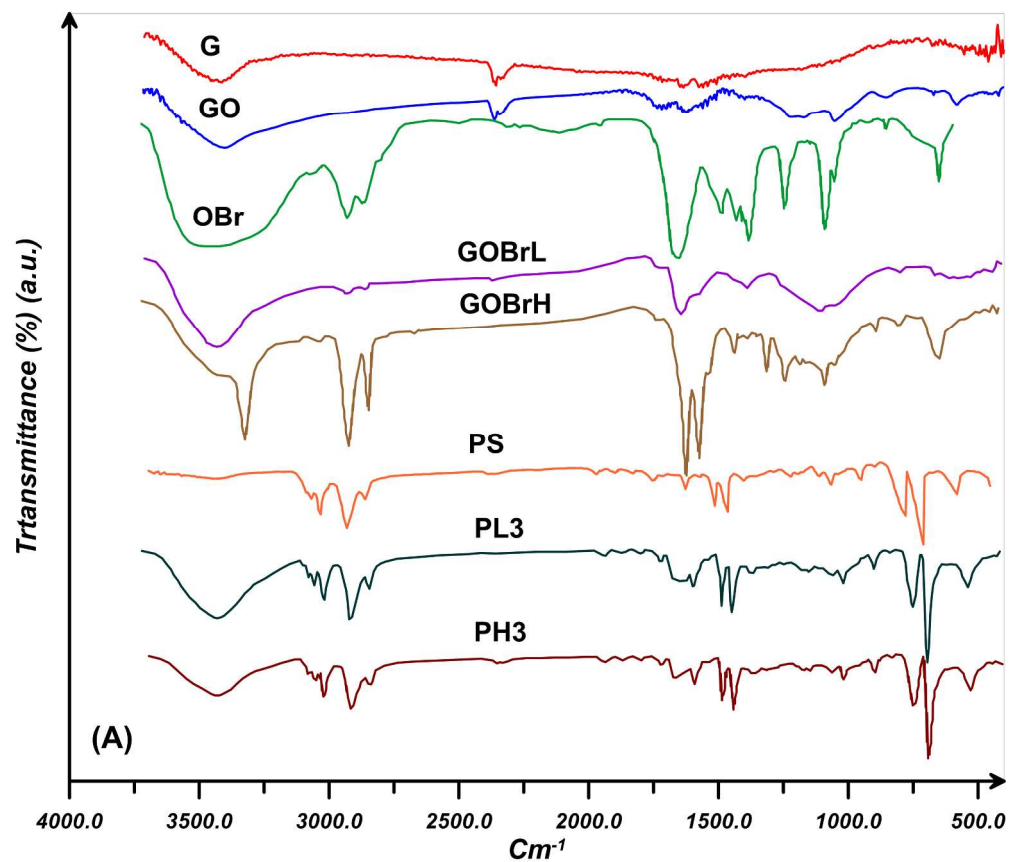


Figure 3- (A) FTIR spectra for the neat and modified graphenes, PS, and its nanocomposites with various graft densities and (B) Raman spectra for graphene, GO, and OBr- and PS-functionalized graphenes with various graft densities
723x621mm (96 x 96 DPI)

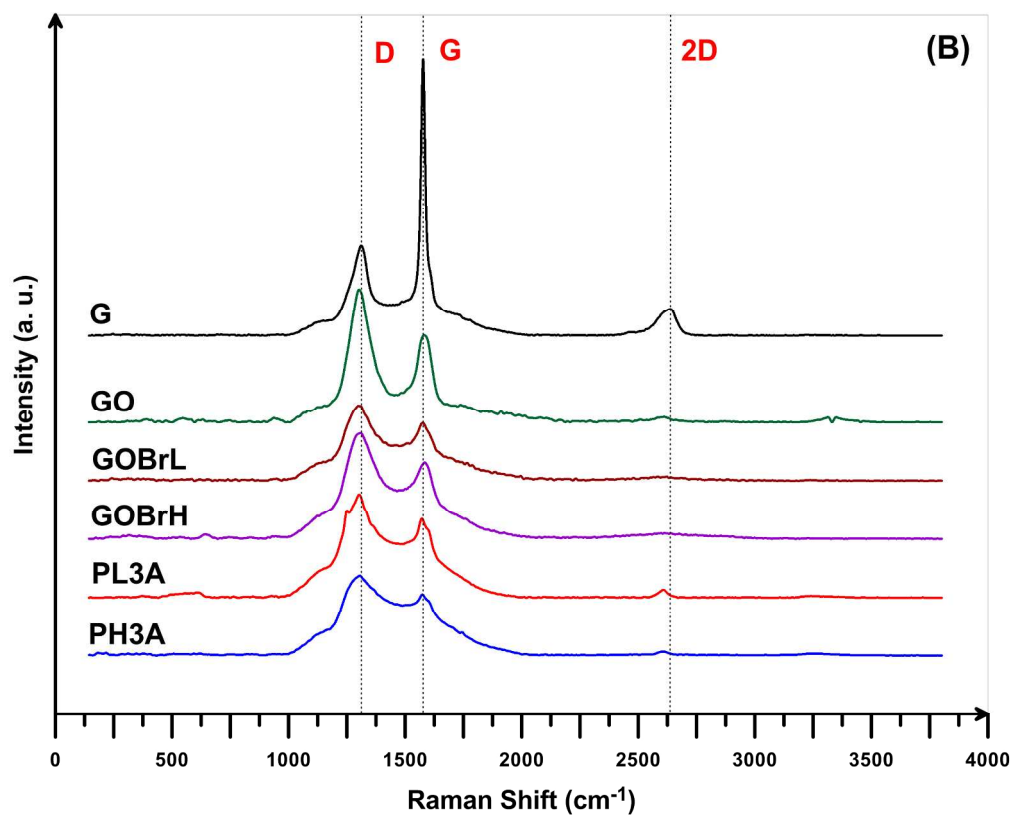


Figure 3- (A) FTIR spectra for the neat and modified graphenes, PS, and its nanocomposites with various graft densities and (B) Raman spectra for graphene, GO, and OBr- and PS-functionalized graphenes with various graft densities
682x549mm (96 x 96 DPI)

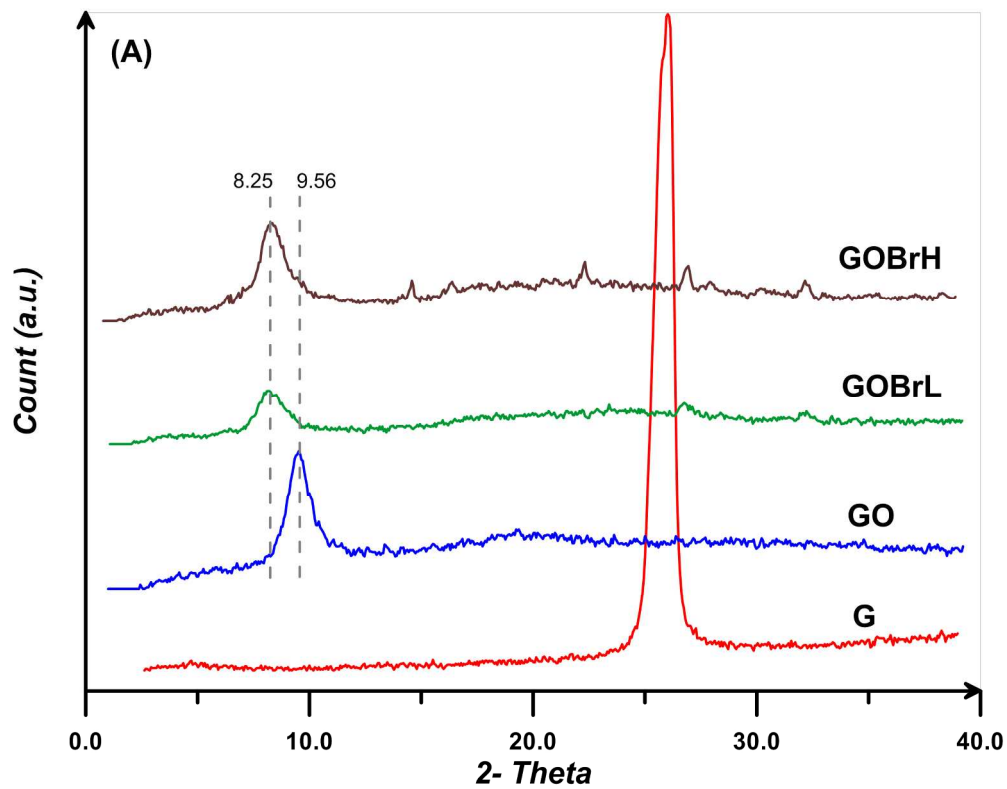


Figure 4- XRD patterns for (A) graphene, GO, GOBrL, and GOBrH and (B) PS nanocomposites with various graft densities
644x506mm (96 x 96 DPI)

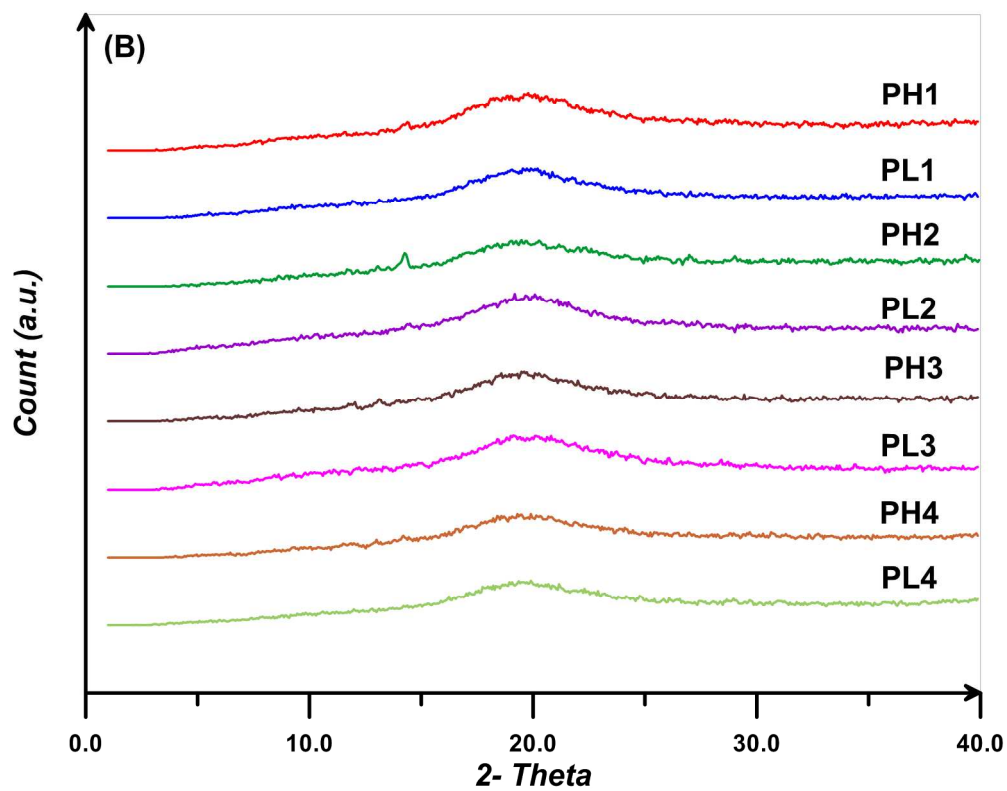


Figure 4- XRD patterns for (A) graphene, GO, GOBrL, and GOBrH and (B) PS nanocomposites with various graft densities
644x506mm (96 x 96 DPI)

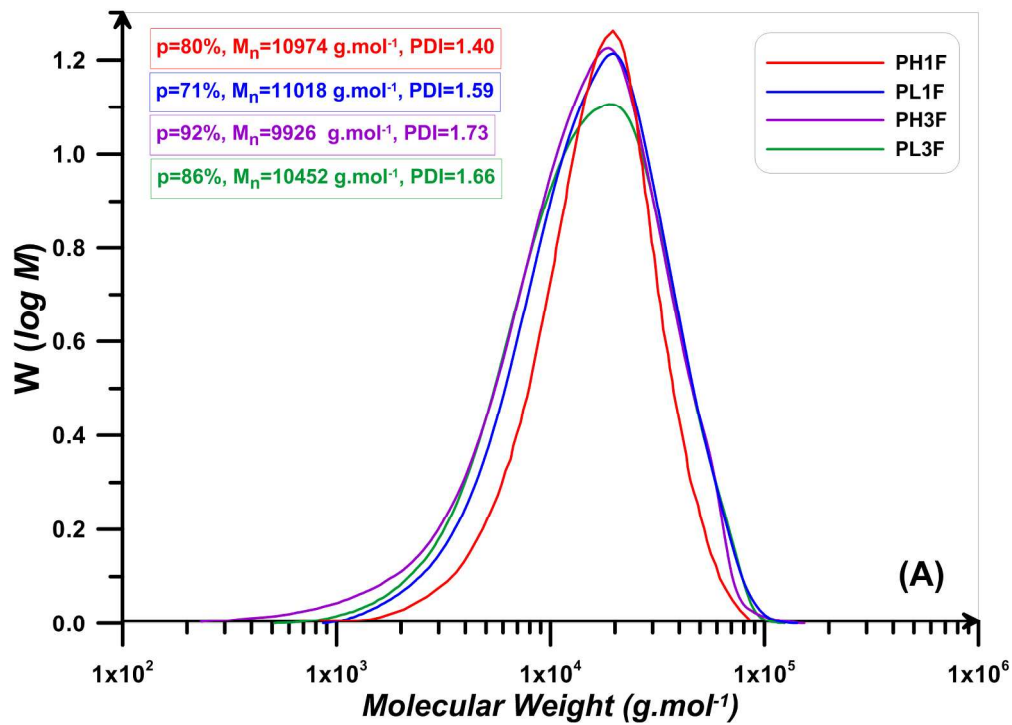


Figure 5- GPC traces for the (A) free and (B) graphene-attached PS chains
650x467mm (96 x 96 DPI)

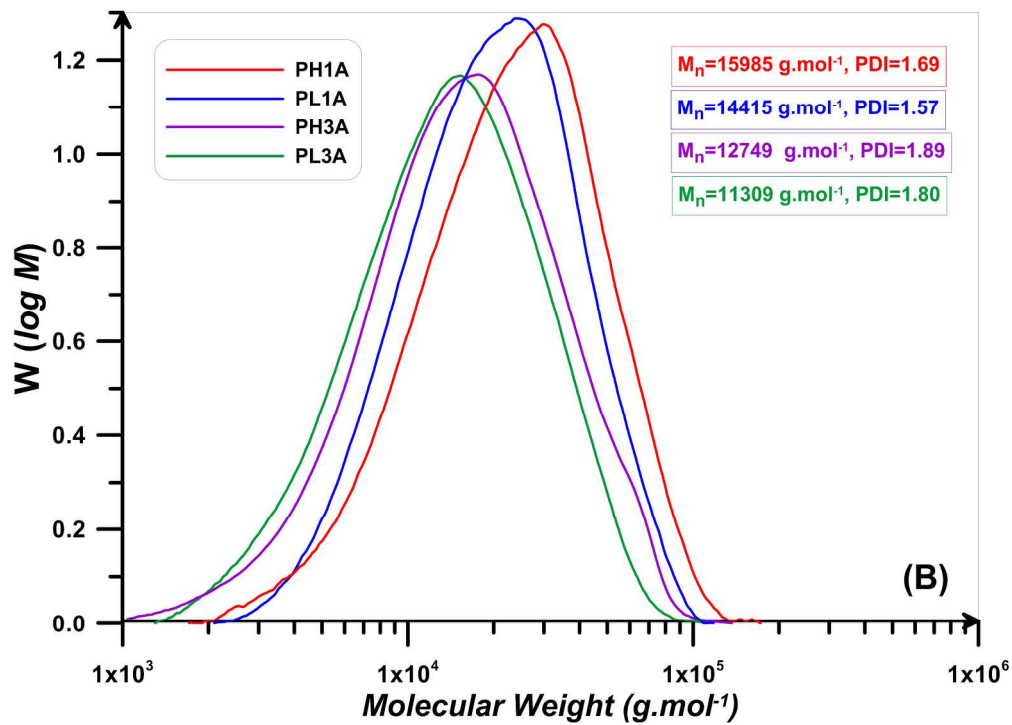


Figure 5- GPC traces for the (A) free and (B) graphene-attached PS chains
650x467mm (96 x 96 DPI)

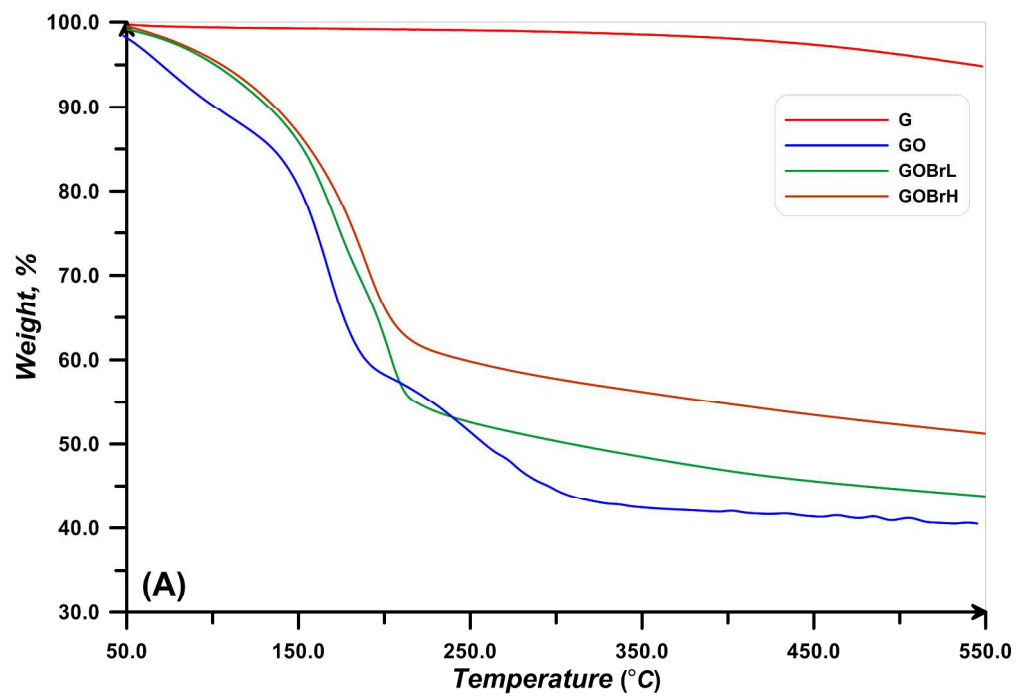


Figure 6- TGA thermograms for (A) neat and modified graphenes, (B) nanocomposites with high graft density, (C) PS-functionalized graphenes with high graft density, and (D) PS-functionalized graphenes with low graft density
740x505mm (96 x 96 DPI)

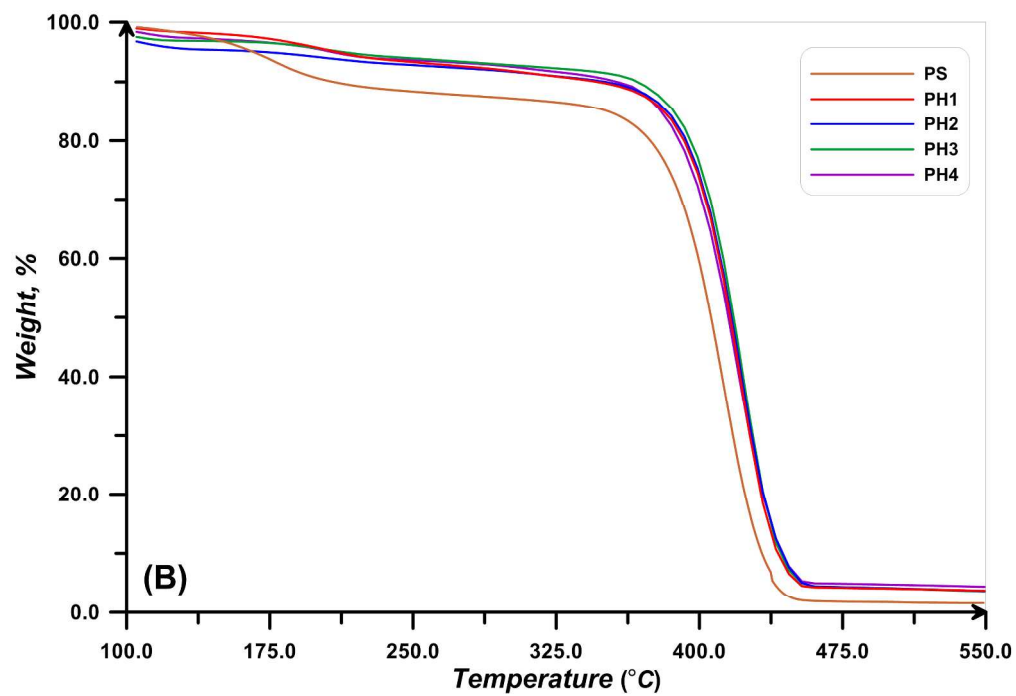


Figure 6- TGA thermograms for (A) neat and modified graphenes, (B) nanocomposites with high graft density, (C) PS-functionalized graphenes with high graft density, and (D) PS-functionalized graphenes with low graft density
740x505mm (96 x 96 DPI)

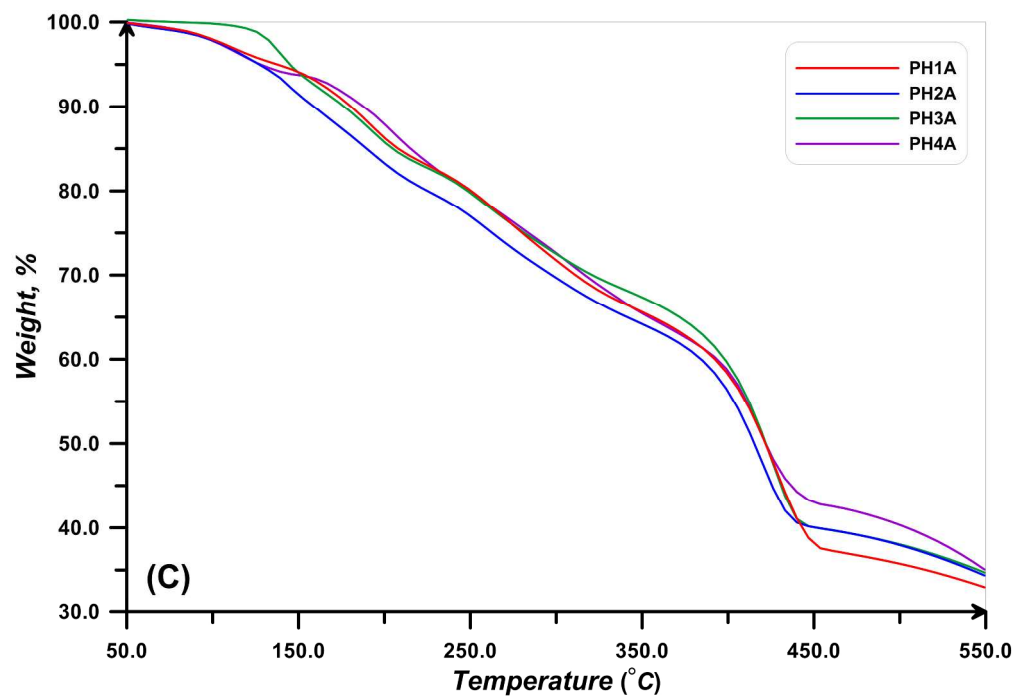


Figure 6- TGA thermograms for (A) neat and modified graphenes, (B) nanocomposites with high graft density, (C) PS-functionalized graphenes with high graft density, and (D) PS-functionalized graphenes with low graft density
740x506mm (96 x 96 DPI)

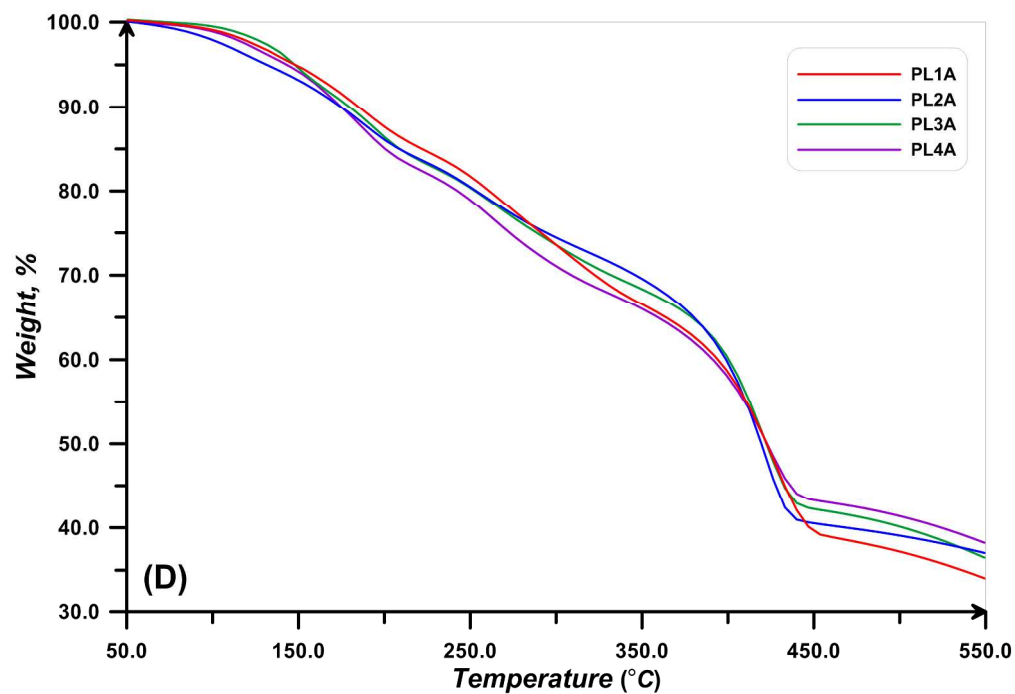


Figure 6- TGA thermograms for (A) neat and modified graphenes, (B) nanocomposites with high graft density, (C) PS-functionalized graphenes with high graft density, and (D) PS-functionalized graphenes with low graft density
740x505mm (96 x 96 DPI)

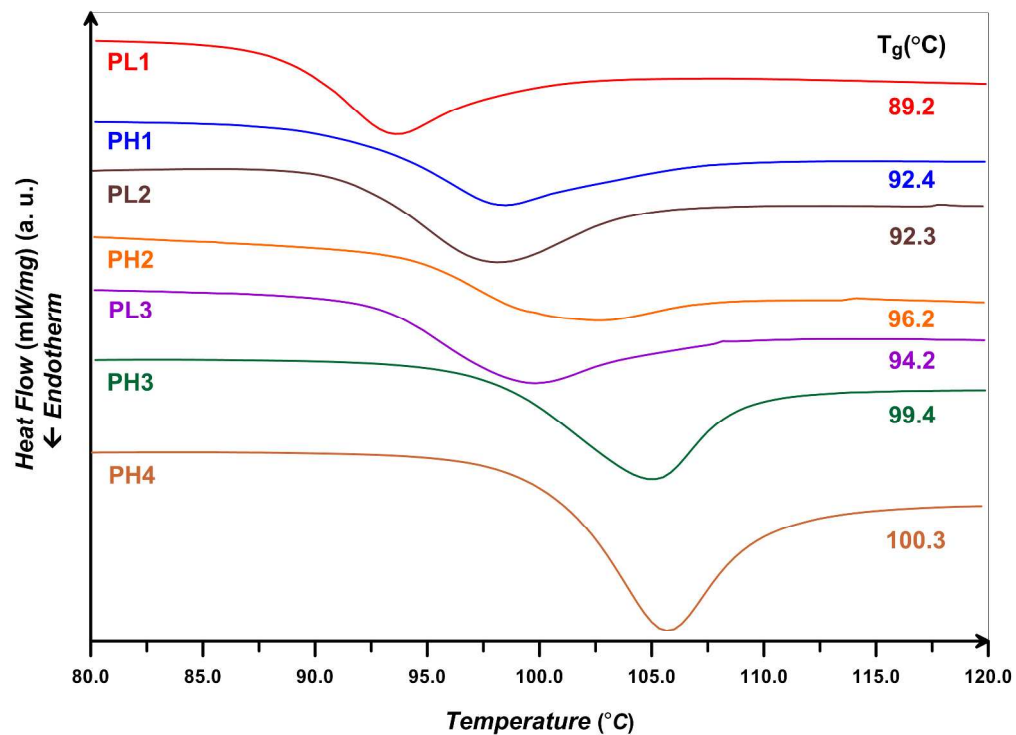


Figure 7- DSC thermograms for PS nanocomposites with various grafting densities
819x597mm (96 x 96 DPI)

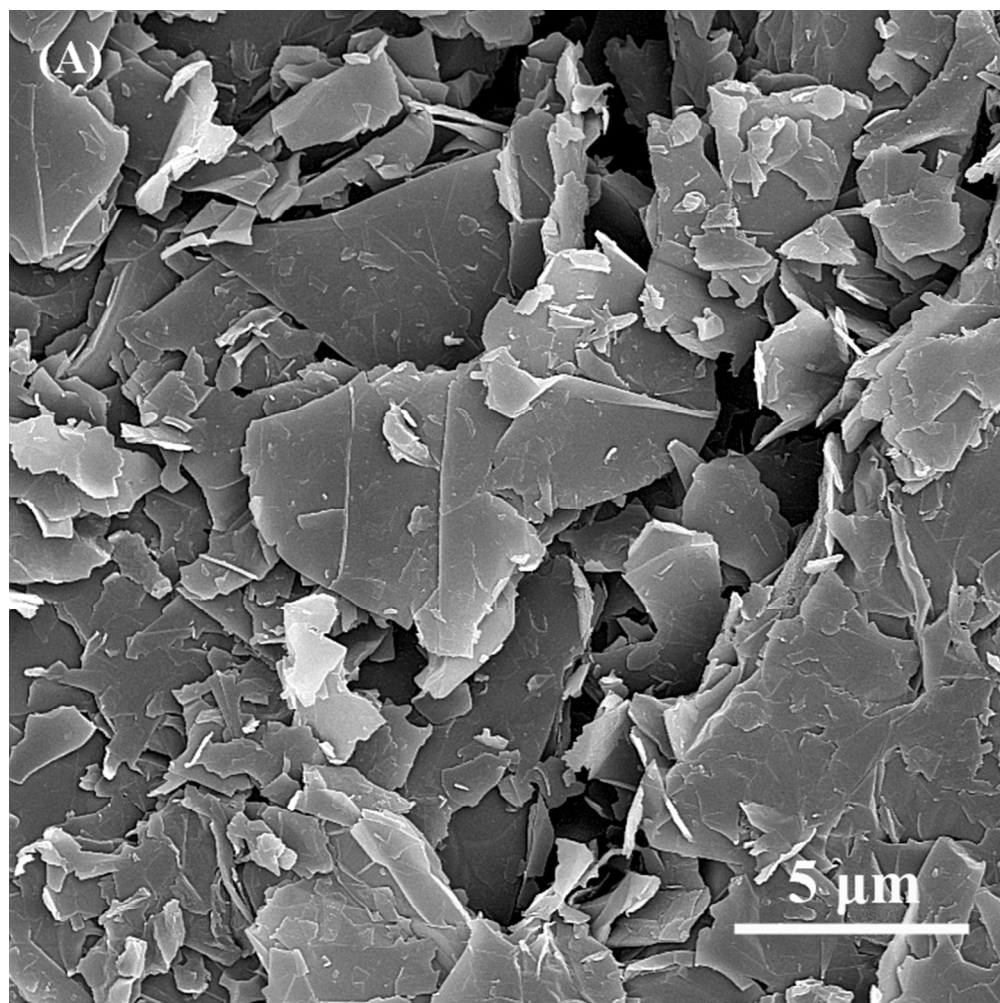


Figure 8- SEM images for (A) graphene, (B) GO, (C) GOBrH, and (D) PH3A, TEM micrograph of (E) graphene and (F) GO, and (G) PH3A, and (H) Dispersion behavior of pristine and surface-modified graphenes in DMF just after sonication and 10 days later
203x202mm (96 x 96 DPI)

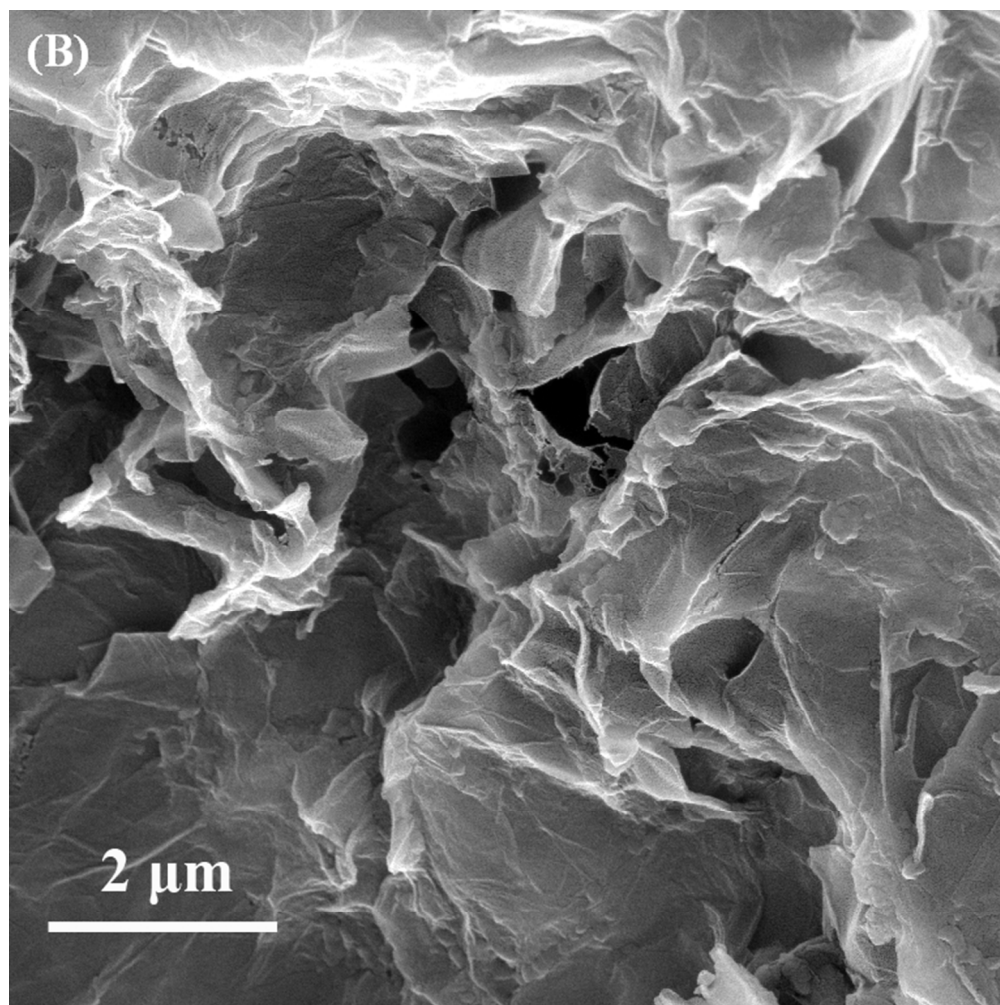


Figure 8- SEM images for (A) graphene, (B) GO, (C) GOBrH, and (D) PH3A, TEM micrograph of (E) graphene and (F) GO, and (G) PH3A, and (H) Dispersion behavior of pristine and surface-modified graphenes in DMF just after sonication and 10 days later
203x203mm (96 x 96 DPI)

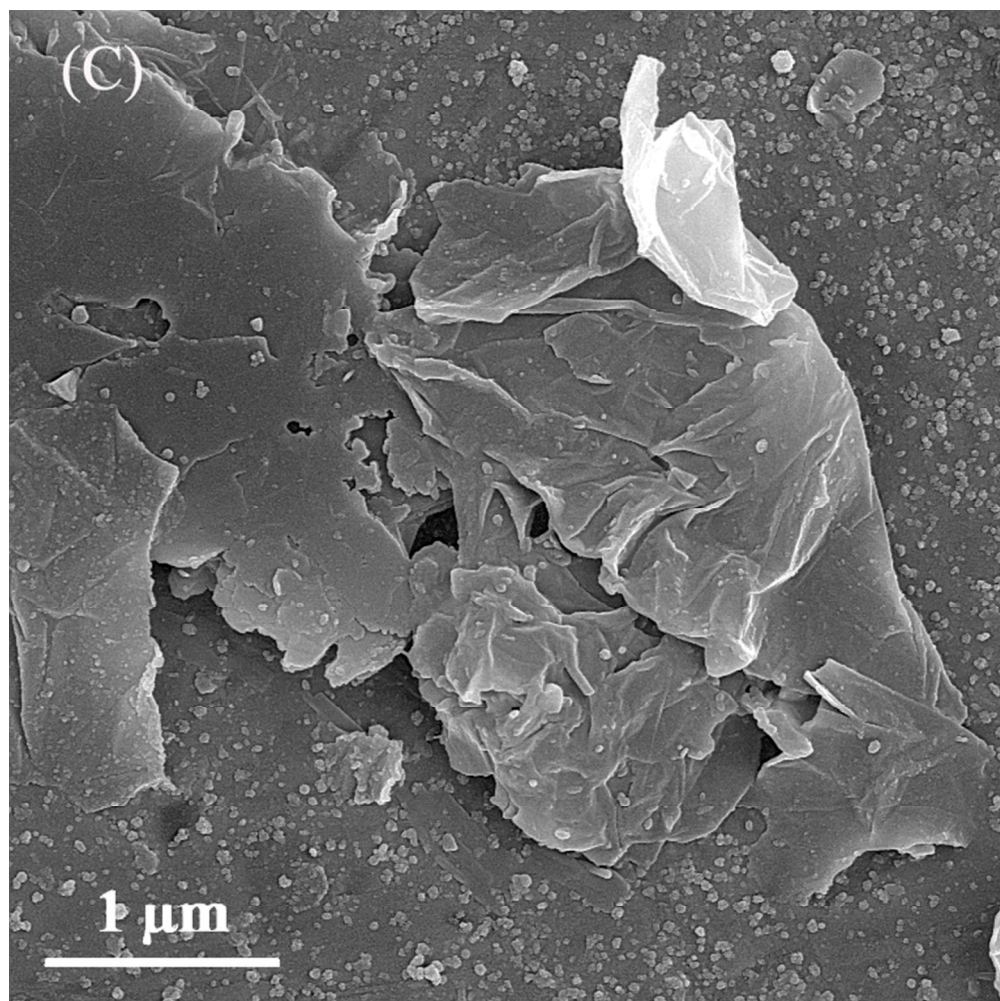


Figure 8- SEM images for (A) graphene, (B) GO, (C) GOBrH, and (D) PH3A, TEM micrograph of (E) graphene and (F) GO, and (G) PH3A, and (H) Dispersion behavior of pristine and surface-modified graphenes in DMF just after sonication and 10 days later
203x202mm (96 x 96 DPI)

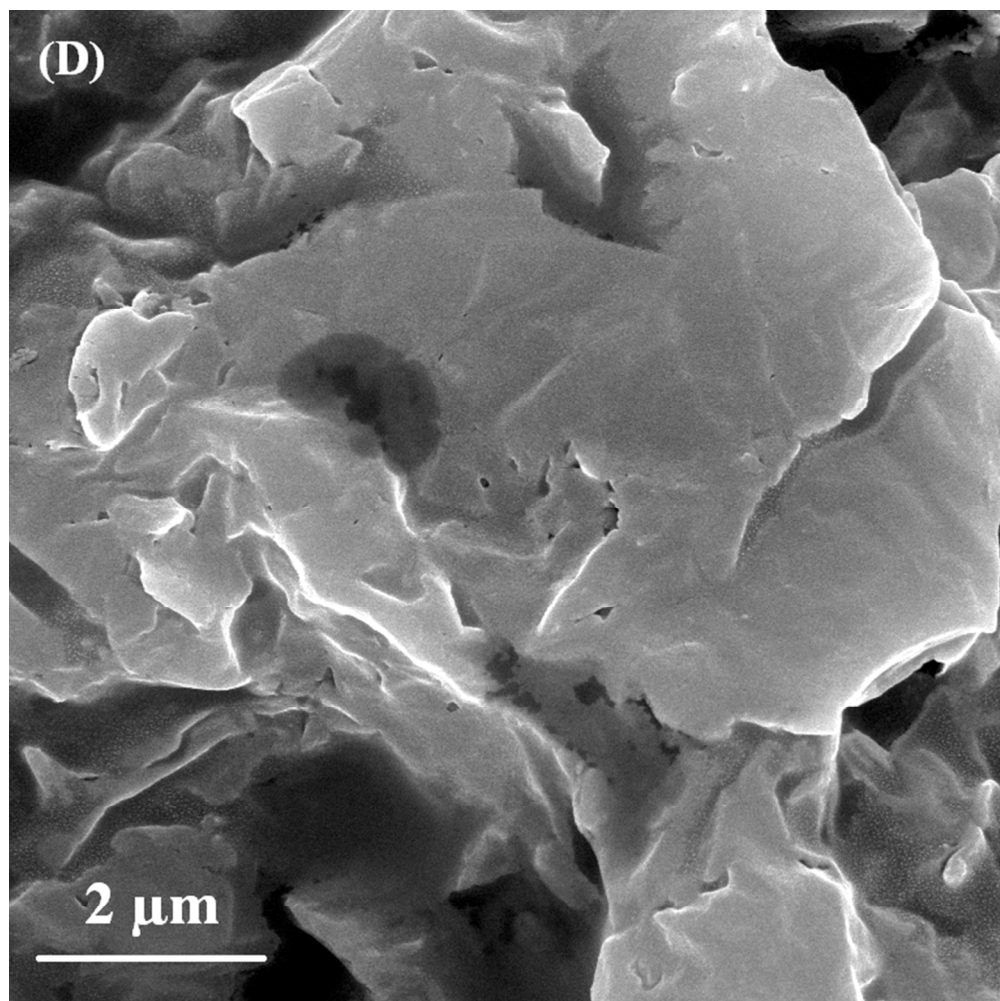


Figure 8- SEM images for (A) graphene, (B) GO, (C) GOBrH, and (D) PH3A, TEM micrograph of (E) graphene and (F) GO, and (G) PH3A, and (H) Dispersion behavior of pristine and surface-modified graphenes in DMF just after sonication and 10 days later
203x202mm (96 x 96 DPI)

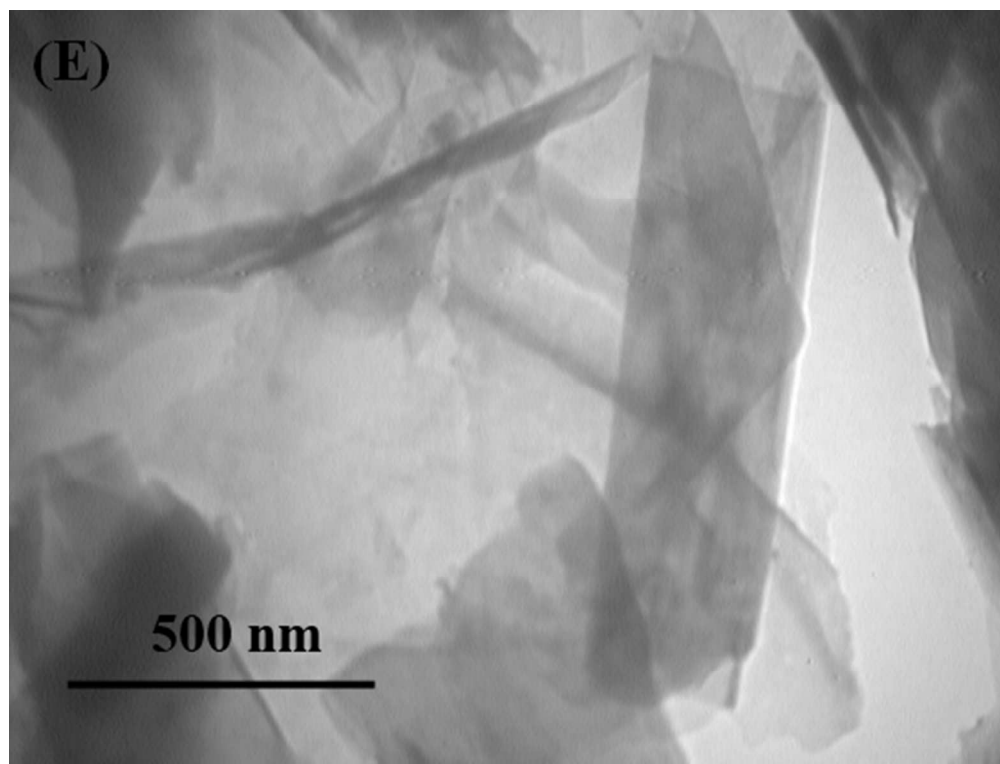


Figure 8- SEM images for (A) graphene, (B) GO, (C) GOBrH, and (D) PH3A, TEM micrograph of (E) graphene and (F) GO, and (G) PH3A, and (H) Dispersion behavior of pristine and surface-modified graphenes in DMF just after sonication and 10 days later
193x146mm (72 x 72 DPI)

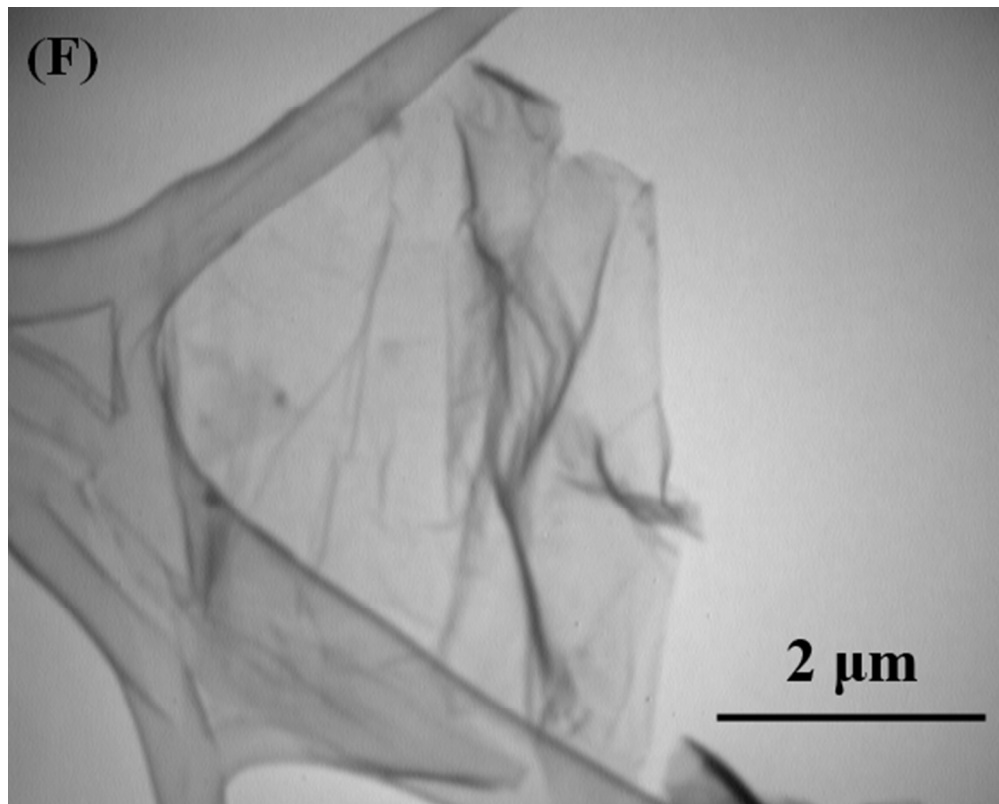


Figure 8- SEM images for (A) graphene, (B) GO, (C) GOBrH, and (D) PH3A, TEM micrograph of (E) graphene and (F) GO, and (G) PH3A, and (H) Dispersion behavior of pristine and surface-modified graphenes in DMF just after sonication and 10 days later
203x163mm (72 x 72 DPI)

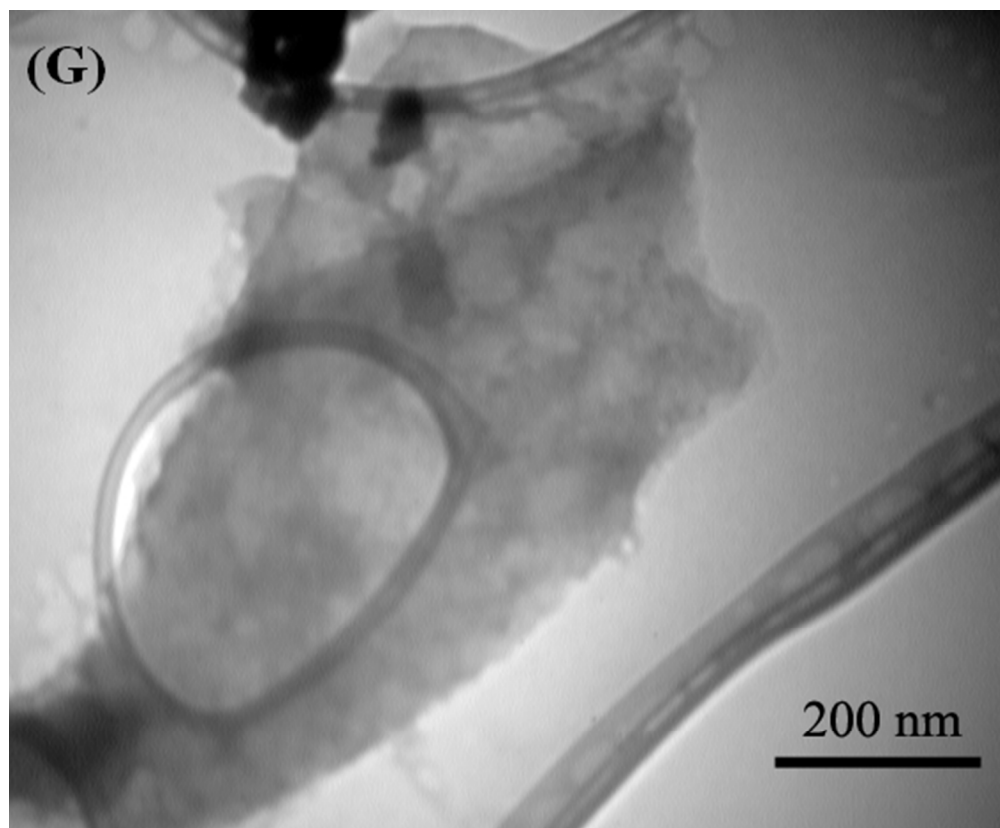


Figure 8- SEM images for (A) graphene, (B) GO, (C) GOBrH, and (D) PH3A, TEM micrograph of (E) graphene and (F) GO, and (G) PH3A, and (H) Dispersion behavior of pristine and surface-modified graphenes in DMF just after sonication and 10 days later
200x165mm (72 x 72 DPI)

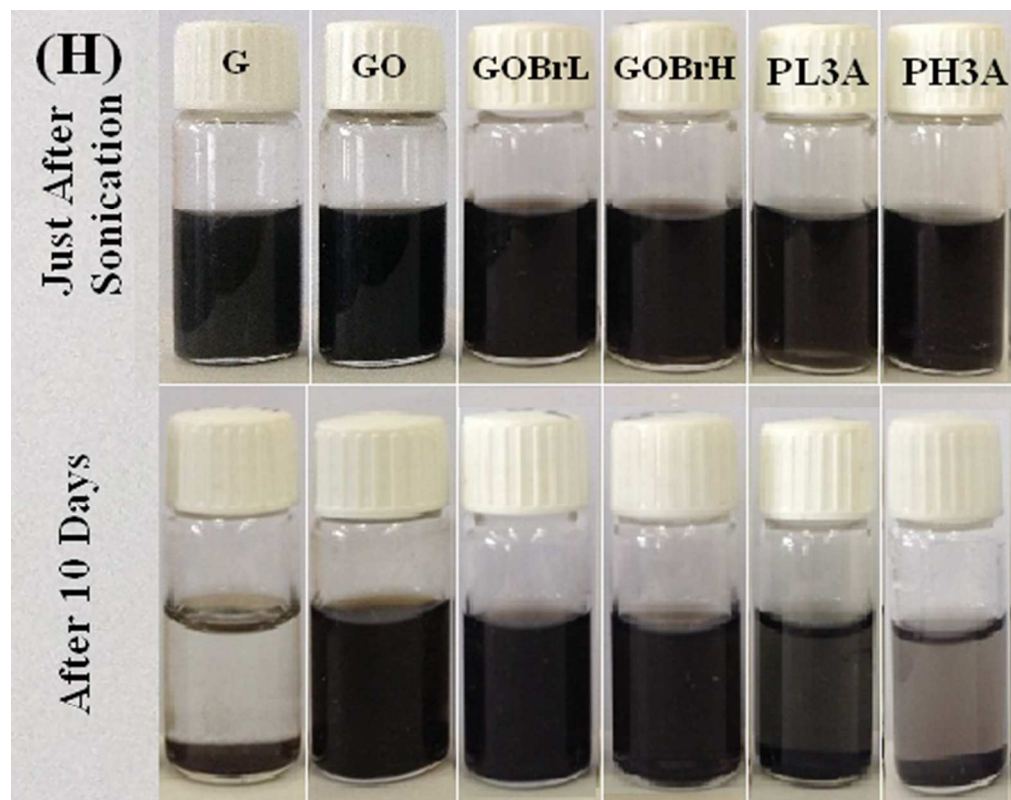


Figure 8- SEM images for (A) graphene, (B) GO, (C) GOBrH, and (D) PH3A, TEM micrograph of (E) graphene and (F) GO, and (G) PH3A, and (H) Dispersion behavior of pristine and surface-modified graphenes in DMF just after sonication and 10 days later
140x111mm (96 x 96 DPI)